

ASTRONOMICAL INSTITUTE  
SLOVAK ACADEMY OF SCIENCES

CONTRIBUTIONS  
OF THE ASTRONOMICAL OBSERVATORY  
SKALNATÉ PLESO

• VOLUME L •

Number 4



November 2020

## Editorial Board

### Editor-in-Chief

Augustín Skopal, *Tatranská Lomnica, The Slovak Republic*

### Managing Editor

Richard Komžík, *Tatranská Lomnica, The Slovak Republic*

### Editors

Drahomír Chochol, *Tatranská Lomnica, The Slovak Republic*

Július Koza, *Tatranská Lomnica, The Slovak Republic*

Aleš Kučera, *Tatranská Lomnica, The Slovak Republic*

Luboš Neslušan, *Tatranská Lomnica, The Slovak Republic*

Vladimír Porubčan, *Bratislava, The Slovak Republic*

Theodor Pribulla, *Tatranská Lomnica, The Slovak Republic*

### Advisory Board

Bernhard Fleck, *Greenbelt, USA*

Arnold Hanslmeier, *Graz, Austria*

Marian Karlický, *Ondřejov, The Czech Republic*

Tanya Ryabchikova, *Moscow, Russia*

Giovanni B. Valsecchi, *Rome, Italy*

Jan Vondrák, *Prague, The Czech Republic*

©

Astronomical Institute of the Slovak Academy of Sciences  
2020

ISSN: 1336–0337 (on-line version)

CODEN: CAOPF8

---

Editorial Office: Astronomical Institute of the Slovak Academy of Sciences  
SK - 059 60 Tatranská Lomnica, The Slovak Republic

# CONTENTS

## STARS

- M.Yu. Skulsky: **Formation of magnetized spatial structures in the Beta Lyrae system. II.** Reflection of magnetically controlled structures in the visible spectrum . . . . . 717
- M.V. Vavrukh, D.V. Dzikovskyi: **Exact solution for the rotating polytropes with index unity, its approximations and some applications** . . . . . 748

## ADDENDUM

**”Universe of Binaries, Binaries in the Universe” Conference  
Telč, Czech Republic, September 7-11, 2019**

- K. Zervas, E.-P. Christopoulou, A. Papageorgiou: **Substellar and stellar companions in eclipsing binaries** . . . . . 772
- A. Papageorgiou, P.-E. Christopoulou, M. Catelan, A.J. Drake, S.G. Djorgovski: **What we can learn from eclipsing binaries in large surveys: The case of EA Catalina systems** . . . . . 774

The Contributions of the Astronomical Observatory Skalnaté Pleso  
are available in a full version  
in the frame of ADS Abstract Service  
and can be downloaded in a usual way from the URL address:

**<https://ui.adsabs.harvard.edu/>**

as well as from the web-site of  
the Astronomical Institute of the Slovak Academy of Sciences  
on the URL address:

**<https://www.astro.sk/caosp/caosp.php>**

The journal is covered/indexed by:

**Thomson Reuters services (ISI)**

Science Citation Index Expanded (also known as SciSearch®)  
Journal Citation Reports/Science Edition

**SCOPUS**

## Formation of magnetized spatial structures in the Beta Lyrae system

### II. Reflection of magnetically controlled structures in the visible spectrum

M.Yu. Skulskyy

*Lviv Polytechnic National University, Department of Physics, 79013, Lviv,  
Ukraine, (E-mail: [mysky@polynet.lviv.ua](mailto:mysky@polynet.lviv.ua))*

Received: April 13, 2020; Accepted: June 9, 2020

**Abstract.** This article proposes a picture of magnetized accretion structures formed during the mass transfer in the Beta Lyrae system. It is shown that the structure of the gaseous flows between the donor and the gainer is due to the spatial configuration of the donor magnetic field. Its dipole axis is deviated substantially from the line joining the centers of the components and is inclined to the orbital plane of the binary system; the center of the magnetic dipole is displaced from the donor center toward the gainer. The surface around the donor magnetic pole, which is close to the gainer, is a region of an additional matter loss from the donor surface. The effective collision of the magnetized plasma with the accretion disk is enhanced by the fast counter-rotation of this disk, especially in the secondary quadrature phases, in which the high-temperature medium and the system of formed accretion flows are observed.

This concept is demonstrated, primarily, in the obvious correlations between the phase variability of the donor magnetic field and the corresponding variability of the dynamic and energy characteristics of the various complex lines. This refers to the behavior of the radial velocity curves of the emission-absorption lines formed in the gaseous structures of type  $H_\alpha$ , He I  $\lambda$  7065, or the variability of their equivalent width and intensity, and the variability of conventional absorption lines of the donor atmosphere. This is true for the phase variability of the absolute flux in the  $H_\alpha$  emission line and the fast varying of the continuum in the  $H_\alpha$  region as certain parameters, which reflect the phase variability of the donor magnetic field. This approach made it possible to determine the phase boundaries of the location of the magnetic polar region on the donor surface above which the matter outflows are formed.

**Key words:** binaries: individual: Beta Lyrae – emission-line: magnetic field: mass-transfer

## 1. Introduction

The previous article (Skulskyy, 2020) was intended to provide an overview and analysis of long-term observations needed to further highlight the questions

aimed primarily on the study of magnetized gaseous structures. This thematic was decisive and intensively developed on the basis of spectral observations on large telescopes with the latest equipment in 1980-1995. Discoveries made in original investigations, such as Skulskij (1985, 1992); Alexeev & Skulskij (1989); Burnashev & Skulskij (1991); Skulskij & Malkov (1992); Skulskij & Plachinda (1993), and others, have allowed us to create a certain picture of magnetized gaseous structures until the mid-1990s. Along with a number of such studies over the next decade, this picture has changed little. The following points should be briefly noted. The analysis of all observations and studies of the donor magnetic field showed that the systematic observations on the 6-m SAO telescope could be considered decisive for the further study of the mass transfer and the formation of accretion structures in the Beta Lyrae system. Based on these observations, in Skulskij (1985) the first simulation of the donor magnetic field configuration was conducted. The axis of the magnetic field is directed by the orbital phases of (0.355-0.855) P. It is also important that the magnetic dipole axis is inclined to the orbit plane of the binary system by an angle of  $28^\circ$ , and the center of the magnetic dipole is displaced by 0.08 of the distance between centers of gravity of both components from the donor center toward the gainer. It could be assumed that the mass loss and its transfer from the donor to the gainer can occur not only in the direction of the (0.5-1.0) P phases of the star-components gravity axis, but also in the direction of the magnetic field axis. That is, in addition to the gas flow that is directed from the deformed donor through a Lagrange point to the gainer's Roche cavity in a classical hydrodynamic picture (see Bisikalo et al., 2000), there is the matter outflow channeled by the donor magnetic field in the direction of its dipole axis from the donor surface and deflects along the magnetic field lines toward the accretion disk. Moreover, the donor magnetic pole in the 0.855 P phase is located on the donor surface slightly above the orbital plane and approximated to the gainer. This presumes also the presence of more effective shock collisions of the magnetized plasma in the phases of the second quadrature (0.60-0.85) P at all heights of the accretion disk. The energy effect of shock collisions of magnetized gas with the accretion disk is amplified in these phases due to the rapid counter-rotation of this disk forming a hot arc on the outer rim of the accretion disk facing the donor, (see Skulsky, 2015, 2018).

These inferences, based on the spatial configuration of the donor magnetic field, required a number of diverse observations and developed gradually. At the same time, other scientists have also pointed out the need for such research. Bahyl (1986), after having carefully studied the spectral absorption lines of the donor atmosphere, noted: "the curve of the systems magnetic field variations is similar in shape to the curves of the phase variations of the equivalent width of the corresponding lines". Aydin et al. (1988) also indicated that the presence in the Beta Lyrae spectrum of the high-temperature resonance lines of NV, Si IV, and CIV implies the existence of non-thermal sources in this system, which cannot be matched by the radiation from stellar components; however, this can be considered in the context of the discovery of a variable magnetic

field by Skulskij (1985). Recently, Ignace et al. (2018), while studying the phase variability of complex emission-absorption profiles of the  $H_\alpha$  line, concluded that in the explanation of the observation data “the magnetic field...could prove relevant, e.g., Skulsky (2018)”.

Our analysis of known published observations has shown that the donor magnetic field is in some way reflected in infrared, optical and UV spectral regions. This has stimulated the detailed investigation of the Beta Lyrae spectrum to present it in the summarized work. This article focuses mainly on the extended study of the continuum and complex lines in the visual spectrum with a view of detecting, understanding, and explanation of the relationships between the phase variability of the donor magnetic field and the characteristics of the physical processes occurring in moving gaseous structures between the donor and the gainer.

It should be recalled that the longitudinal component of the donor’s magnetic field changes significantly during the orbital period (which is close to 12.94 d); phase changes in the range from zero to one, being tied to the main minimum of this binary system in the visible spectral region when the more massive accretor obscures of the bright donor; the schematic model of the Beta Lyrae system and the picture of mass transfer are shown in Skulskyy (2020) in Figure 1, which is needed to understand the physical processes in further analysis.

## 2. Magnetic field and physical processes in gaseous structures between donor and gainer

### 2.1. Magnetic field and the absolute flux in $H_\alpha$ emission line

The first among the most important results on the radiation of accretion flows in the Beta Lyrae system was obtained by Burnashev & Skulskij (1991) on the basis of their spectrophotometry that was carried out in 1974-1985. The narrowband photometry was given in values of the monochromatic illuminance at the top of the Earth’s atmosphere  $\log E(\lambda)$  in  $erg \cdot sec^{-1} \cdot cm^{-2}$  at a 1-cm wavelength interval. Along the continuous spectrum of this binary system the wavelengths of the important selected working bands were  $\lambda\lambda$  6488, 6563, and 6637. The absolute flux in the  $H_\alpha$  emission line above the continuous spectrum in the band  $\lambda$  6563 was considered as a certain physical parameter in view of the interconnection to the variable magnetic field of the donor. Incidentally, the monochromatic light curve reflecting the radiation flux in the band at  $\lambda$  6488 showed that in the second quadrature the binary system is hotter than in the first one. This brightening in the continuum correlates with such excess in the far-ultraviolet (Kondo et al., 1994). However, the dependence of the absolute radiation flux  $E(H_\alpha)$  on the orbital phase is more interesting (see Fig. 1) and needs more careful consideration.

The upper box in Fig. 1 shows the variation of the effective magnetic field of the donor as calculated from measurements made on Zeeman spectrograms in

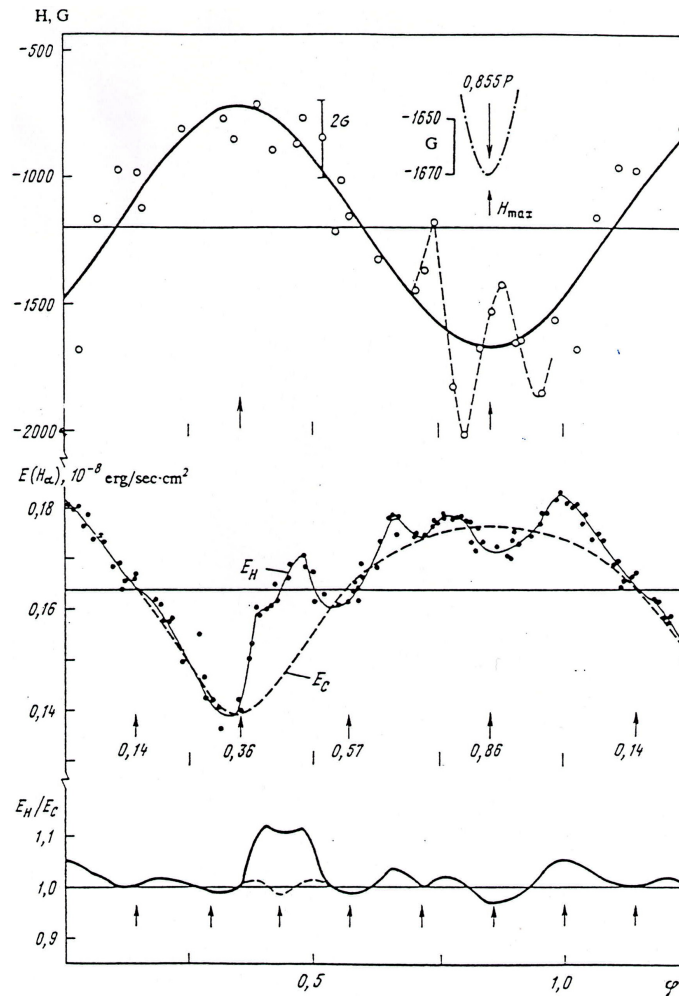


**Figure 1.** At the top - the variability over the orbital phase of the effective magnetic field strength of the donor; in the middle - the variability over the orbital phase of the absolute radiation flux in the  $H_\alpha$  emission line; bottom - the 12% increase in the radiation flux in the  $H_\alpha$  emission line in the phases round 0.43 P, which is interpreted as a result shock collisions of gaseous flows with the accretion disk. (Burnashev & Skulskij, 1991).

1980-88. This quasi sinusoidal curve shows the maximum value of the magnetic field of negative polarity at the phases around 0.855 P (the characteristic time of its secondary variations one also can see at these phases). The dipole axis in direction (0.355-0.855) P has the 0.145 P position-angle deviation (one-seventh

of the orbital period) from the line joining the centers of stars in the binary system in the direction (0.5-1.0) P. In the center of Fig. 1 the solid line, denoted  $E_H$  represents  $E(H_\alpha)$  as a function of phase. This dependence was derived from the observation points obtained by moving the phase interval of 0.07 P in steps of 0.01 P. The average error per point is less than  $\sigma = 0.03 \cdot 10^{-8} \text{ erg/cm}^2 \cdot \text{sec}$ . Figure 1 clearly shows that the minimum and maximum values of the radiation flux in the  $H_\alpha$  line correspond to the two phases of the extreme values of the magnetic field of the donor. It is seen that the phase variability of the radiation flux of the  $H_\alpha$  line has a narrow minimum coinciding in phase with the magnetic field minimum, and the broad maximum of the radiation flux in the  $H_\alpha$  line matches with the phase of the maximum value of the magnetic field. The phase intervals of the minimum  $\Delta P_{min}=(0.57 \text{ P}-0.14 \text{ P})$  and maximum  $\Delta P_{max}=(1.14 \text{ P}-0.57 \text{ P})$  of the radiation flux of the  $H_\alpha$  line have the ratio close to 3/4. The radiation flux in the  $H_\alpha$  emission line between these extremes of the magnetic field increases 1.3 times, having some constant minimum level in the phase of the minimum of the donor magnetic field.

From this, it can be concluded that if the Roche cavity of the donor is filled, as is generally accepted, it should be assumed that the outermost layers of the donor surface easily lose matter in the direction of the dipole axis of (0.355-0.855) P. However, this is observed mainly from the donor surface in the phase region around 0.855 P, i.e., in phases of the observation of the magnetic field pole facing the gainer. The radiating matter, as a material leaving the donor in the form of a stellar wind along the lines of the magnetic field, deflects hereafter to the gainer and forms a complex structure of accretion flows. And since initially the gas moves perpendicularly to the donor surface, the  $H_\alpha$  emission line is generated close to the donor surface and its averaged radial velocities must first have a thermal component, that is, they should not be very large Skulskij & Malkov (1992). This is confirmed in section 2.3, where the radial velocity of the  $H_\alpha$  emission line as a whole shows the variability over the orbital period in the range of  $\pm 45$  km/s.

Another non-trivial, but expected, result was obtained. The solid line middlemost in Fig. 1 shows, that there is the variable radiation flux of the  $H_\alpha$  line at the maximum of the magnetic field, but there is also its explicit excessively outstanding part at the phases of (0.36-0.51) P that makes apparent the additional  $H_\alpha$  line radiation flux (by 12 percent relative to the smoothed  $E_c$  curve; see Fig. 1, bottom). The phase interval with the width of  $\Delta P=0.15$  P can be interpreted as the localization zone of direct collisions of gas flows with the accretion disk at the formation of a hot region on it. This is confirmed by numerous polarimetric Beta Lyrae observations, including those of Appenzeller & Hiltner (1967); Hoffman et al. (1998), and Lomax et al. (2012) where all polarization curves show a pronounced minimum at the phases near 0.47 P, which is interpreted as a result of enhanced scattering by free electrons near the accretion disk. This is also confirmed by the modeling of the light curve by Mennickent & Djurašević (2013) with the detection at the phases around 0.40 P of the hotter

region located on the accretion disk. However, the absolute spectrophotometry by Burnashev & Skulskij (1991) identified clearly both the center and the phase boundaries ( $0.43 \pm 0.06$ ) P of the hotter region projected onto the accretion disk.

Hence, the absolute spectrophotometry of the Beta Lyrae system revealed the fact of the apparent synchronous variability over the orbital phase of both the effective magnetic field strength of the donor and the absolute radiation flux in the  $H_\alpha$  emission line. This indicates that the donor magnetic field directly reflects the processes of radiation generation in the formed under its influence spatial magnetized gaseous structures at the mass transfer in this binary system.

## 2.2. Magnetic field and the rapid variability of the spectrum in the $H_\alpha$ emission region

The foregoing result is confirmed by a study of Alexeev & Skulskij (1989) of the ultra-fast variability of the Beta Lyrae spectrum in the region of the  $H_\alpha$  emission line. Observations of this binary system were conducted for 8 nights (over a 13-day orbital period) in August of 1981, using the 6-m SAO telescope in conjunction with the dissector spectrophotometer. The spectral range investigated, centered on  $H_\alpha$  for two dispersions amounting to 0.6 and 0.9 Å/channel respectively, was 150 Å and 460 Å. The accumulation time for an individual spectrum was equal to 10.48 and 5.24 seconds, respectively. All the data were obtained with a spectral resolution of 0.6 Å/channel. Only at the 0.73 P phase did we make observations using two different options. Based on processing over 700 individual spectra, one should focus on three original results.

The first important result is the detection of an unusually wide base emission under the strong emission peak in the  $H_\alpha$  line that is known to have a height of several continuums and a total width of up to 700 km/s. This broad base emission component has the total width above 6000 km/s, whereas photographic spectral observations, for example by Batten & Sahade (1973), show that such a broad component of the  $H_\alpha$  emission is only of 1000 km/s. The highest dome-shaped substrate of the broad emission component over 3000 km/s wide rises at its center above the continuum to 25% in the 0.34 P phase, up to 30% in the 0.73 P phase, and up to 17% in the 0.87 P phase, that is in the phases of both quadratures near observation phases of both poles of the magnetic field (see Figure 2 as the fragment of Figure 13 from the article of Alexeev & Skulskij (1989)). On the averaged spectrum with the spectral range of 460 Å at the 0.73 P phase (88 single spectra), in addition to the  $H_\alpha$  line, the He I  $\lambda$  6678 emission line was also present, which made it possible to more reliably mark the continuum level. On the violet side of the broad emission component, the narrow absorption with a radial velocity above -2000 km/s is observed in the phase 0.73 P in the two averaged spectra with the spectral ranges 150 Å and 460 Å, respectively, and also the absorption at -1000 km/s in the phases 0.34 P and 0.49 P. This may indicate high-velocity gas jets from a binary system that are observed in phases near both poles of the magnetic field.

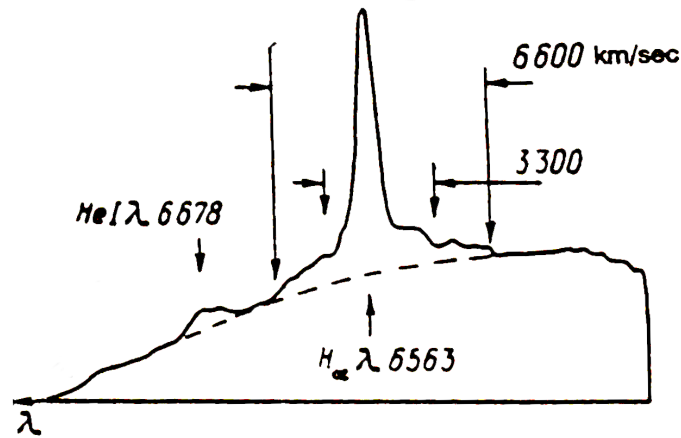


**Figure 2.** An average Beta Lyrae spectrum in relative intensities in the 0.73 P phase (series of spectra with lower spectral resolution): the continuum level under  $H_{\alpha}$  is indicated by the dashed line.

The high speeds of motion of the radiating atoms, which follow from the fact of the detection of intensive and broad wings of an  $H_{\alpha}$  emission line in quadratures, indicate that the space between the donor and the accretion disk is the zone of the localization of the high-temperature hydrogen medium and of the shock collisions of the speeded-up flows with this disk. The smallest contribution to the continuum in the range of the broad emission component, in particular their distant wings, is observed at phases 0.03 P, 0.11 P close to the donor eclipse when the red wing is practically absent (in other words, the high-temperature radiating gas is here almost completely obscured by the accretion disk and only a small amount of this gas moves above this disk in the direction of the gainer, i.e., toward the observer).

The second important result relates to the rapid variability of spectrum in the  $H_{\alpha}$  line region, which shows significant differences over the orbital phase. The time intervals of this variability range from seconds to tens of minutes. The least emission flux variability is observed in the main minimum at the 0.03 P phase. There is no appreciable variability in this flux at the 0.88 P and 0.11 P phases that are close and symmetric relative to the donor eclipse or the primary minimum of the binary system. In these three phases, the observation region of presumed collisions of the gaseous flows with the disk surrounding the gainer is almost completely eclipsed by this accretion disk (see Figure 1 in Skulsky (2020)). However, shifting along the positional angle of the observation of the binary system, in particular at the 0.34 P, 0.42 P, and 0.49 P phases, the variability of the radiating flux in the  $H_{\alpha}$  emission line increases substantially: both in the shape and intensity of the central emission peak, as well as within

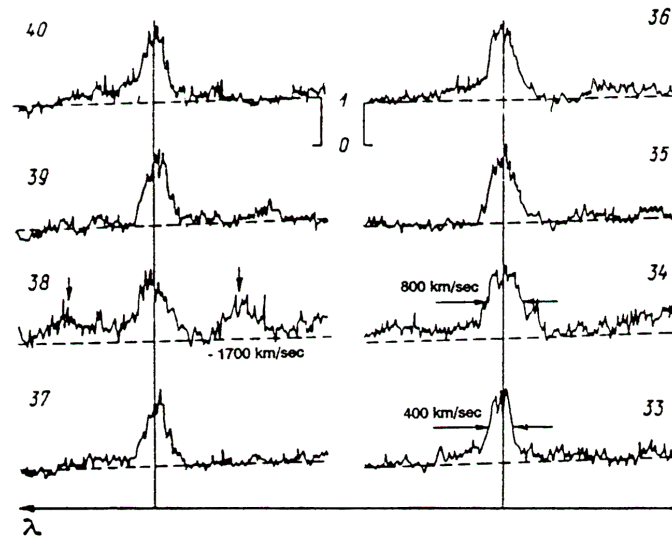


**Figure 3.** An example of quantitative estimates on single 10-second H $\alpha$  line spectra in the 0.49 P phase: the height of the continuum is shown on spectra 36 and 40; on spectra 33, 34, and 38 there are indicated kinematic estimates of variable details of the spectrum. (Alexeev & Skulskij, 1989)

the width of the emission component around this peak. At the 0.34 P phase, when the space between the components of the binary system is still visible, there is relatively little variability over the entire 15-minute observation. Here, the monotonous variability of the central two-peak profile of the H $\alpha$  emission line was observed, with fast changes for several one-minute intervals. In the next phase of 0.42 P, i.e., in the phase of observing the known hot region of the accretion disk, the chaotic variability of the entire emission on 10-second spectra increased very significantly, in both the central peak of the H $\alpha$  emission line and its broad emission component. However, the most intensive variability of unusual modifications in the entire investigation region of the spectrum near the H $\alpha$  emission line is observed in the 0.49 P phase.

The evidence of obtained fast changes in the vicinity of the H $\alpha$  line in the 0.49 P phase is shown in Fig. 3, which is a copy of Figure 23 from the article of Alexeev & Skulskij (1989). Time intervals of the continuous variability of different details in this spectrum diapason are observed from seconds to ten minutes. This result is not simple to understand because at the 0.49 P phase the donor should practically eclipse the known hot region on the accretion disk. At the same time, from the space around this hot region, the gas outflow moves with a great radial velocity of about -1000 km/s, which is recorded in the spectrum by the appearance of absorption lines at phases from 0.34 P to 0.49 P. Then, it is

possible to assume the formation of the hot pulsating plasma at the upper disk region, not obscured by the donor, as a result of the collision in this region of ionized gas channeled toward the accretion disk due to the specific structure of the donor magnetic field (the magnetic dipole axis is inclined to the orbit plane of this binary system by an angle of  $28^\circ$ ). This may indicate that the moving gas passing along the lines of the magnetic field in the direction of the gainer collides with the accretion disk not so much in the plane of the orbit as the entire height of the disk, forming in front of the disk some scattering structures, which are clearly shown in Figure 1 as the hotter region on phases (0.39-0.51) P. It should be considered that the visible height of the accretion disk in phases of active shock collides may be observed above the donor surface.

The third result is similar to the phenomenon of the eruptive nature, which consists of two components: “emission flare-up” and “traveling absorption”. It was recorded in the set of 49 spectra at phase 0.81 P and is shown in Figures 24-28 of Alexeev & Skulskij (1989). The development of the central part of this phenomenon is illustrated in Fig. 4, which is a copy of Figure 28 from Alexeev & Skulskij (1989). Initially, from the first to the 31st single spectrum, an unusually low ratio of the flux intensity in the central peak of  $H_\alpha$  emission line to the emission flux intensity in the continuum near the line of  $I_l/I_c$  was observed. This ratio gradually increased from 0.25 to 0.37, but in spectrum 32 reached sharply the value of 0.97, and in 33-49 spectra remained stable at the level of 1.40. Such a sudden increase in the  $I_l/I_c$  ratio in limits 31-33 spectra looked like the “emission flare-up” phenomenon. Such a sharp transformation in the intensity of the  $H_\alpha$  emission line was parallel preceded by the phenomenon of “traveling absorption”, which occurred suddenly within a minute in spectra from 27 to 32. This event began in spectrum 27 with the occurrence of the violet shift absorption at an averaged radial velocity of -2700 km/s from the center of the  $H_\alpha$  line. The core of this absorption, over 2000 km/s wide, reached a depth of 16% in the spectrum 30 and lowered the entire  $H_\alpha$  emission line almost under the continuum. The rapid spectral shift of this absorption along the continuum reached the position of +1100 km/s on the red wing of the  $H_\alpha$  emission line and disappeared almost entirely in the spectrum 32.

The observed phenomenon has no analog, and it is difficult to unambiguously interpret. Its initial stage was fixed at the moment when the spectral region with the central emission peak of the  $H_\alpha$  line had an unusually small contrast with respect to the close continuum ( $I_l/I_c = 0.25$  for the first 2-3 minutes from all 8 minutes observations) and was practically imperceptible unlike the formation region of the broad emission component of this line. It is unknown how long this situation lasted before our observations began (it can be noted that it took at least 5 minutes to verify the correctness of the spectral region identification due to the unusualness of the spectrum near  $H_\alpha$  line). The emergence, development, and disappearance of this peculiar “traveling absorption” at its motion along the continuum (within one minute) can be a reflection of a certain mechanism of the matter ejection in the direction of the observer and the reverse movement of

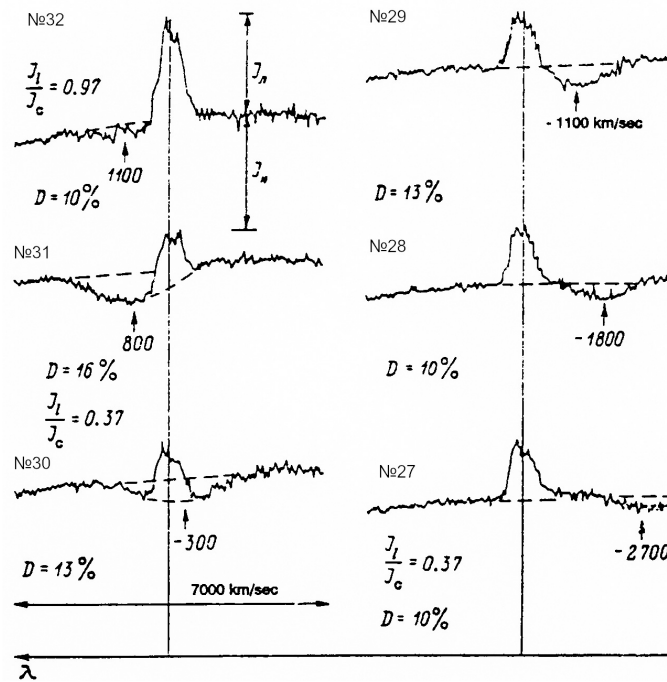


**Figure 4.** Detailed illustration and quantitative characteristics of “traveling absorption” and “emission flare-up” phenomena (dashed lines indicate the behavior of continuum; the zeros of the continuums coincide with the maxima of the lower spectra). (Alexeev & Skulskij, 1989)

this matter of smaller density to the donor surface. This was accompanied by the “emission flare-up” phenomenon, i.e., the sudden (within half a minute) increase in the  $I_l/I_c$  ratio from 0.37 to 1.40 in the central emission peak. However, the characteristic time scale of the variability in the radiation flux of these emissions does not reflect the large-scale motion of gaseous structures commensurate with the Beta Lyrae system.

The aforementioned phenomenon as the event of the eruptive nature may be related to the spatial configuration of the donor magnetic field. Indeed, this phenomenon was detected at the 0.81 P phase when the pole of the magnetic field on the donor surface is directed towards the observer (incidentally, Skulskij (1982) observed the maximum of the magnetic field of the donor on the 6-m SAO telescope the same night in August of 1981). This phenomenon is more likely to have local spatial and temporal characteristics close to the donor surface. Such an event may be a reflection of the ejection of a matter directly from the donor surface, on which the location of the magnetic field pole, close to the gainer, is

clearly visible in this phase. That is, this event may reflect the motion of magnetically controlled matter, which can be directed outward from the magnetic polar region on the donor surface, as suggested by Shore & Brown (1990) for helium stars. This is also just one of the possible spatiotemporal events of different durations recorded by different observers, for example, Bless et al. (1976); Skulskij (1980). It is confirmed by Kondo et al. (1994) owing to the observed outburst fixed on the 965 Å band light curve in the same second quadrature. The physical nature of such events may be similar. It can be assumed that the ionized plasma, which is channeled by the magnetic field of the donor from its surface and subsequently collides with the accretion disk, is not laminar, but is accompanied by sometimes significant non-stationary ejections.

### 2.3. Magnetic field, dynamics of the $H_\alpha$ emission line and other emission-absorption lines

From foregoing convincing correlations between the variability of the radiation flux in the  $H_\alpha$  line and the effective magnetic field strength of the donor, the logical task was to investigate such causal relationships based on the dynamics and structure of the complex  $H_\alpha$  emission line. It should be noted that our long-term studies of strong hydrogen and helium emission lines, starting with Skulskij (1972), have shown that the variability of these lines required obtaining better spectral material. The exact emission-absorption profiles of the  $H_\alpha$  lines, represented on a dynamic scale as “relative intensity versus radial velocity” according to Figure 2 of Skulskij & Malkov (1992), were obtained using high-dispersion 3 and 6 Å/mm CCD spectrograms for 20 nights 1985-1990 on the 2.6-m CrAO telescope. This article confirmed the reality of both the rare sharp fluctuations in the  $H_\alpha$  flux at intervals of up to 10 minutes and some of the seasonal changes noted in previous studies. More importantly, this article presented the new results of reliable measurements of the Doppler shifts of the structural components of the  $H_\alpha$ -profile, as well as the factors affecting the profile and dynamics of the  $H_\alpha$  emission line as a whole.

The  $H_\alpha$  emission line, as the strongest emission line of the visible spectrum of the Beta Lyrae, exhibits two emission peaks above the continuum and the absorption feature between these emission peaks. The radial velocities of these three variable structural components are traditionally measured. Skulskij & Malkov (1992) measured these line components based on the hypothesis that the  $H_\alpha$  emission line as a whole is of a common nature and that the absorption component, which cuts through this emission, originates as self-absorption in this emission line. Under this hypothesis of Skulskij & Malkov (1992), the radial velocities of the Gaussian center of the total emission as a whole were also measured. The measurements of the radial velocities of structural components of the  $H_\alpha$  line showed that all four radial-velocity curves are in one way or another correlated with the effective magnetic field curve of the donor over the orbital period (see Figure 5 of Skulskij & Malkov (1992)). Two types of the

$V_r$ -curves are identified: 1) those that more clearly correlated with the radial velocity curves of the components of the binary system, i.e., related in space to the line of their centers, which passes through the direction of the phases of (0.5-1.0) P; and 2) those that more clearly correlated with extrema of the effective magnetic field of the donor, i.e., with the spatial direction of the dipole axis of its magnetic field of (0.355-0.855) P (see Figure 1). The first type of curve is the radial velocity curve of the absorption feature, which shows negative radial velocities at all phases reflecting the gas flows motion. The radial velocity curve for the Gaussian center of the  $H_\alpha$  emission is definitely of the other type: both its maxima clearly match extrema of the effective magnetic field strength of the donor. Hence, such an approach to the measurement of Doppler shifts of the characteristic features of the  $H_\alpha$  emission-absorption line as a function of the orbital phase has revealed two major factors forming its shape and dynamics. The more important one reflects the Doppler phase shifts of the  $H_\alpha$  emission profile as a whole. It follows that the generation of the radiation flux in the  $H_\alpha$  emission line and the formation of the emission-absorption profile of this line can be formed under the certain influence of the donor magnetosphere.

These results changed the understanding of the formation of gas structures and required confirmation. Therefore, in the following year, 1991, the intensive CCD observations of the Beta Lyrae in the red spectral range were extended. They included the simultaneous detailed study of general regularities in the phase variability of the parameters of emission-absorption lines  $H_\alpha$ , He I  $\lambda\lambda$  6678, 7065 and Si II  $\lambda\lambda$  6347, 6371. The investigation of circumstellar structures and mass transfer in the presence of the donor magnetic field, which was based on a study of the dynamical and energy characteristics of these lines, is given by Skulskij (1993a). Figure 5, which is presented here as Figure 3 from Skulskij (1993a), shows quite sufficient statistical reliability of the four radial velocity curves of the components of the  $H_\alpha$  emission line, which were obtained with the incorporation of the data from Skulskij & Malkov (1992). Figure 5 illustrates also the phase coordination of these radial velocity curves with the curve of the effective magnetic field of the donor (see Fig.1) that needs careful consideration.

First of all, in Fig. 5, the measurements of the Doppler shifts of the  $H_\alpha$  profile components are presented separately for 1985-89 and 1990-91. In the later period, clear differences in the radial velocity curves of the blueshifted (or violet) peak are revealed, indicating certain long-term changes in the gas emitting structures directed mainly to the observer. These changes are observed in phases (0.0-0.15) P, but especially in phases from 0.50 P to 0.75 P of the second quadrature (see Fig. 5, bottom). The shape of this curve is clearly changed in 1990-91 at a virtually invariable shape of the radial velocity curve of the absorption component that points out the independence of the moving plasma radiated in the violet emission peak. Indeed, the minimum value of negative radial velocity fell from -100 km/s to -50 km/s diminishing accordingly the distance in radial velocities between the violet and red emission peaks, and the width of the  $H_\alpha$  emission as a whole. Moreover, the violet emission peak shifted

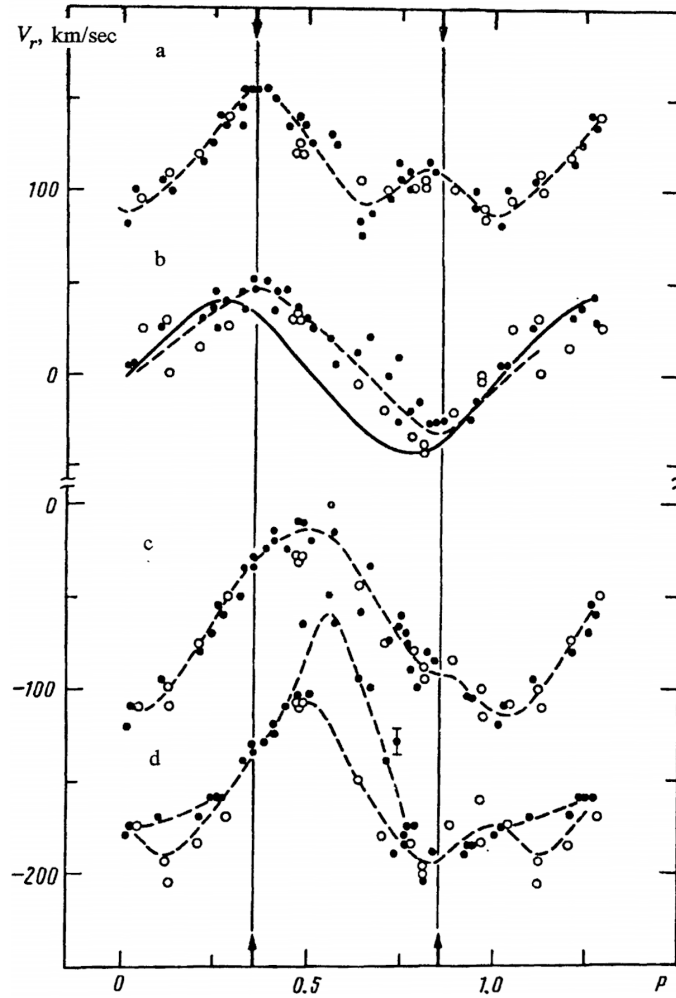


**Figure 5.** Radial-velocity curves of structural components of the  $H_{\alpha}$  emission profile based on CCD observations in 1990-91 (dots) and 1985-89 (circles) for: a) the redshifted peak; b) the center of the Gaussian profile  $H_{\alpha}$  emission (the solid curve is the  $V_r$  curve for the gainer); c) the absorption feature cutting through the emission; d) the blueshifted peak (the mean error  $\approx 2\sigma$  of an individual measurement is shown by a vertical bar). The dashed curves were drawn by hand. The zero points on the vertical axis coincide with the zero velocity of the binary system's center of mass. Two extrema of the curve of the effective magnetic field strength are marked by arrows and vertical lines at the phases 0.355 P and 0.855 P. (Skulskij, 1993a)

to the phases of (0.55-0.60) P, reflecting a certain direction perpendicular to the direction of the axis of the donor magnetic field of (0.35-0.85) P. It is important that during all the years at the 0.85 P phase, which corresponds to the phases of the maximum magnitude of the donor magnetic field and the visibility of the magnetic field (see also Fig. 1), this violet peak shows the maximum value of the negative radial velocity of -200 km/s. It could be interpreted as the additional matter outflow from the region of the magnetic field pole of the donor surface, facing the gainer, along the direction of the magnetic field axis of (0.35-0.85) P.

A clear correlation is observed between the radial velocity curves of the star-components of the binary system and the radial velocity curve of the absorption on  $H_\alpha$  emission profile. This almost symmetric  $V_r$ -curve with the shape of a dome around the 0.55 P phase shows here the minimum radial velocity of -15 km/s of matter in the direction from the binary system. This is close to the thermal velocity from the surface of the bright donor that reaches to its Roche cavity. At the phases of both quadratures, the radial velocity of the outflowing matter reaches -80 km/s. The radial velocity curve becomes slightly asymmetric at the 0.85 P phase of the magnetic field maximum and shows the maximum of negative velocities near -115 km/s (close to the parabolic velocity of the moving gas) at the 0.05 P phase when the stellar wind is converted into the fast flow up to the backside of the accretion disk. Both lower  $V_r$ -curves in Fig. 5 reflect also the spatial structure of the binary system: they are almost symmetrical about the line of centers of its components, which passes through the phases of 0.5 P and 1.0 P. However, the two extrema of these curves reproduce the direction of the phases close to (0.6-1.1) P, i.e., the spatial line that is turned on a quarter of the orbital period relative to the dipole axis of the donor magnetic field. This factor should also be taken into account in the study of moving magnetized accretional structures.

The radial velocity curves for the Gaussian center of  $H_\alpha$  emission for 1985-89 and 1990-91 are definitely of the other type: both maxima of this sine curve clearly correspond to two maxima of the curve of the effective magnetic field strength of the donor (see also Fig. 1), indicating that these two curves are physically related. The radial velocity curve of the  $H_\alpha$  emission center is clearly shifted by 0.1 P from the radial velocity curve of the gainer (see Fig. 5). The radial velocity curve for the more intense red emission peak has also maxima at those phases. It should be noted that the low local maximum in the  $V_r$ -curve of this red peak at the 0.85 P phase becomes dominant if one constructs the dependence  $\Delta V_r = f(P)$ , where  $\Delta V_r$  is the difference between the radial velocities of the long-wavelength peak and the center of  $H_\alpha$  emission (see Skulskij & Malkov (1992)). Both upper  $V_r$ -curves in Fig. 5 reflect the phase variability of the donor magnetic field, whose dipole axis is directed along the line of the (0.355-0.855) P phases, i. e., the general emission as a whole and the red peak as components of the  $H_\alpha$  emission-absorption line are essentially formed in the agreement with the spatial configuration of the donor magnetic field.

The foregoing should be considered in conjunction with the careful work of

Sahade et al. (1959). The Beta Lyrae spectrum in  $\lambda\lambda$  3680-4580 was studied on the basis of spectrograms obtained on the Mount Wilson 100-inch reflector. The radial velocities of red emission peaks have been measured in lines of He I  $\lambda\lambda$  3888, 4472 and  $H_\gamma$  line. They are plotted in Figures 18, 19 and 20 of Sahade et al. (1959). These radial velocity curves are in good agreement with the radial velocity curve of the red peak in the  $H_\alpha$  line that is shown in Fig. 5. This is especially true of the two maxima in the radial velocity curve of the strong red peak in the He I  $\lambda$  3888 line. They clearly correspond to the phases of the two extrema on the curve of the effective magnetic field strength of the donor and phases of the visibility centers of two magnetic poles on the donor surface. Such coincidence factors are logical. Their interconnection seems indisputable.

Similar conclusions can be drawn from the consideration of Fig. 6, reproduced from Figure 4 in Skulskij (1993a), as to analogous components in the emission-absorption lines of He I  $\lambda\lambda$  6678, 7065 and Si II  $\lambda\lambda$  6347, 6371 (mainly based on CCD observations in 1991). Indeed, these  $V_r$ -curves have extremal values near certain phases of the orbital period: 0.0 P and 0.5 P, as well as 0.35 P and 0.85 P, i. e., are related to the geometry of the eclipsing binary system and the dipole structure of the donor magnetic field. The orbitally modulated  $V_r$ -curves of these absorption features have practically sinusoidal symmetry with regard to the axis of the gravity centers of both components. Only such  $V_r$ -curve for the He I  $\lambda$  7065 line is shifted somewhat to the left, to the 0.35 P phase, which coincides with the phase of the observation of the donor magnetic pole. Reaching a positive radial velocity of more than +15 km/s here, this  $V_r$ -curve remains positive within (0.3-0.6) P. This new fact indicates that the outflows of the radiating plasma with the thermal velocity from the donor surface along the donor axis from the observer is observed here, i.e., beginning in the direction of the 0.85 P phase of the second magnetic pole and with the next deviation to the gainer. Such matter outflows showed also in the triplet helium line and are probably raised above a denser stream of mainly hydrogen plasma, but reflected primarily in the absorption feature of the  $H_\alpha$  line. The influence of the magnetic field at the 0.85 P phase is clearly visible both on the shape of all absorption  $V_r$ -curves in Fig. 6 and in the absorption feature of the  $H_\alpha$  emission line in Fig. 5.

Comparing Fig. 5 and 6, one should note good agreement between the average  $V_r$ -curves for the emission centers of the  $H_\alpha$  line and lines He I  $\lambda\lambda$  6678, 7065 and Si II  $\lambda\lambda$  6347, 6371. The He I  $\lambda$  6678 line exhibits the greatest uncertainty when measuring radial velocities due to the substantial asymmetry of the emission profile. However, the radial velocities of the powerful He I  $\lambda$  7065 line, whose double-peaked emission, like that of  $H_\alpha$  line, is observed considerably above the continuum over the orbital period, are measured reliably. Together with the radial velocities of the emission centers of the red silicon doublet lines (their values were taken from Skulskij (1992)) they mimic well the average  $V_r$ -curve of the center of  $H_\alpha$  emission as a whole. Thus, two sinusoidal extrema of these dependences  $V_r = f(P)$  coincide (see Fig. 5b and Fig. 6a) with the phases

of passing through the meridian of both poles of the magnetic field on the donor surface (see also Figure 1 in Skulskyy (2020)). In general, it reasonably suggests that the emission and absorption components of these studied lines are produced with almost the same dynamics in gaseous structures between components of this binary system, correlating clearly in orbital phases with the variability of the donor magnetic field.

In view of the above, it is worth noting the thorough work of Harmanec et al. (1996), which, in particular, presents the results of the processing of the electronic spectra obtained in 1992 and 1994 on the reflectors of Ondrejov and Dominion Astrophysical Observatories in the red spectral range 6100-6700Å. Using also the data of our publications (Skulskij, 1972, 1993a; Skulskij & Malkov, 1992), they presented statistically better radial velocity curves of the  $H_\alpha$  emission line for all four of its components (see Figures 8 and 9 in Harmanec et al. (1996)). Their behavior of  $V_r = f(P)$  or “RV curves”, as expected, are in full agreement with the corresponding radial velocity curves in Fig. 5 and 6 of this paper. Their “RV curves of the  $H_\alpha$  and He I  $\lambda$  6678 absorption cores versus orbital phase” show also the minimum -15 km/s and maximum -113 km/s of the negative velocities near the 0.55 P and 0.05 P phases, respectively. The extrema of their RV curves for both emission peaks of the  $H_\alpha$  line clearly correspond to the phases of the observation of the poles of the donor magnetic field or the direction (0.355-0.855) P. Incidentally, the same maximum negative velocity of -200 km/s was shown for the violet emission peak (or “V-peak”) in the 0.855 P phase. These investigators indicate that “the  $H_\alpha$  emission as whole moves almost in anti-phase” to the donor, such that for the radial velocity curve of this emission “the RV minimum is 0.853 P (instead of 0.75 P for the donor)”. This coincides with the maximum of the donor magnetic field at the 0.855 P phase (see Fig. 1), as it follows from the solution of the magnetic field variability curve by Burnashev & Skulskij (1991). And this corresponds to the phase meridian of the passage of the magnetic field pole on the donor surface. It should be noted that in interpreting the Beta Lyrae system Harmanec et al. (1996) do not use such a clear match in these results and the studies of the donor magnetic field as a whole. They concluded: “the bulk of the  $H_\alpha$  and He I  $\lambda$  6678 emission seems to originate in jets of material perpendicular to the orbital plane of the binary”. Here these jets are associated mainly with the gainer and also “probably emanate from the hot spot in the disk, i.e. the region of the interaction of the gas stream flowing from the Roche-lobe filling” of the donor. On the contrary, Ignace et al. (2018) are hopeful that the magnetic field “could prove relevant”. Based on the study and simulating of  $H_\alpha$  line profile variations in the Beta Lyrae spectrum, they have shown that “a circumbinary envelope, a hot spot on the accretion disk, or accretion stream” non-satisfactory explain the observation data. They even presume: “evaluating the detailed radiative transfer for a model involving both a disk and a jet is unlikely to help”.

An important conclusion that the emission as a whole is produced mainly in structures that are affected by the magnetic field, that is, they are largely

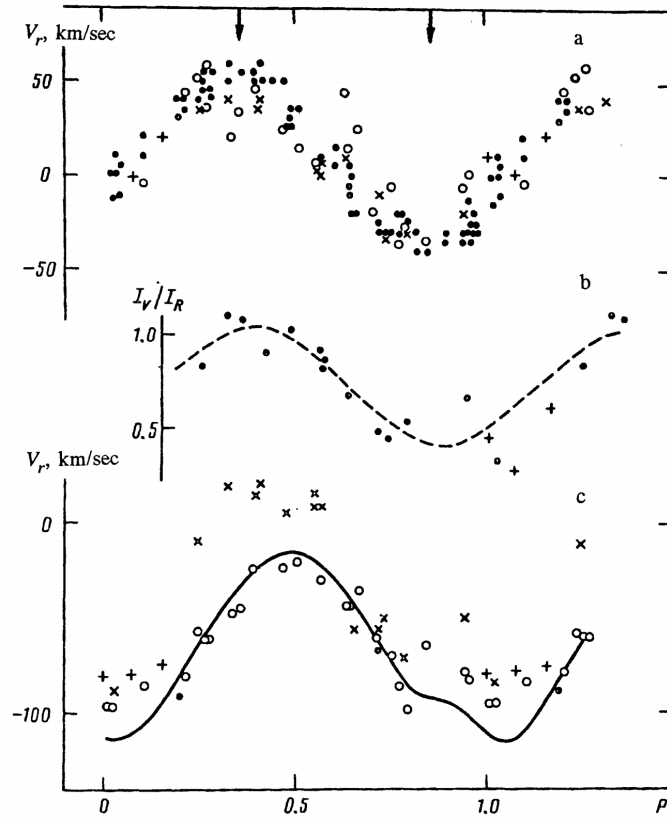


**Figure 6.** Radial-velocity curves of a) the center of the Gaussian emission profile in the Si II  $\lambda\lambda$  6347, 6371 doublet lines (dots), the He I  $\lambda$  6678 line (circles), and the He I  $\lambda$  7065 line ( $\times$ ), supplemented by the 1992 observations (crosses); c) absorption features in the same helium lines (1992 observations in the He I  $\lambda$  7065 line are represented by crosses and the He I  $\lambda$  5875 line are represented by dots); the solid curve here corresponds to the  $V_r$ -curve of the absorption feature in the  $H_\alpha$  line from Fig. 5; b) the  $I_V/I_R = f(P)$  curve for emission in the He I  $\lambda$  7065 line, supplemented by the 1992 observations (crosses). Two extrema of the curve of the effective magnetic field are indicated (at the top) by arrows at the phases 0.355 P and 0.855 P. (Skulskij, 1993a).

generated near the donor surface, was given by Skulskij (1993b,c). This was also based on variations of  $V_r$ -curves of the emission center Si II  $\lambda\lambda$  6347, 6371 lines in 1990-92. There are two irrefutable facts to such conclusion: a shift near 0.1 P in the phase of the  $V_r$ -curve of this emission as a whole, and a shift of about +10 km/s of the center of the radial velocity of this  $V_r$ -curve relative to the

radial velocity of the mass center of the binary system. These factors should be considered based on Fig. 5 and 6. First, a clear difference of 10 km/s between the radial velocity of the mass center of the binary system and the velocity of the emission center of all  $V_r$ -curves implies a constant outflow of matter from the binary system. Then it is necessary to associate this outflow of matter not with the gainer but with the bright donor, which is “constantly expanding” toward its inner Roche cavity. The matter drains essentially and along the magnetic field lines from the donor surface near the magnetic pole facing the gainer, i.e., near the 0.85 P phase (see Figure 1 of Skulskyy (2020)). The maximum negative shift of radial velocities of -45 km/s in the  $V_r$ -curves of the emission centers of all the investigated lines is detected at just those phases (i. e., the motion from the surface of the donor toward the observer). The maximum positive shift of these radial velocities of +45 km/s is recorded in the vicinity of the opposite magnetic field pole around the 0.35 P phases, i.e., the emitting gas moves from the observer (probably along the magnetic field lines), but in the same direction as its the motion registered around the 0.85 P phases. That confirms that gas outflows are produced mainly on the donor surface near the donor’s magnetic pole, which is close to the massive gainer and observes near the 0.85 P phase. At the same time, the  $V_r$ -curves of the emission centers of all the investigated lines are shifted in phase by 0.1 P relative to the  $V_r$ -curve of the gainer, and the sinusoidal maxima of these  $V_r$ -curves coincide with such maxima on the curve of the donor magnetic field (see also Fig. 1). This is strong evidence of the physical relationship between the regions of spatial formation of the total emission and the structure of the donor magnetic field. One can also consider as reasonable the picture, in which the magnetized plasma, moving from the donor surface mainly in the 0.85 P phases and deflecting afterward to the gainer, forms a system of gas flows directed toward the accretion disk (this is also seen from the radial velocity curve of the absorption component of the  $H_\alpha$  emission line).

Hence, it should be stressed that the variability of the complex profiles of the emission-absorption lines over the orbital period, in terms of their dynamic characteristics, is essentially synchronous with such variability of the magnetic field of the donor. The reflection of accretion flows in the spectrum of this interacting binary system during the mass transfer from the donor to the gainer is largely determined by the existing spatial structure of the magnetic field of the donor.

#### **2.4. Magnetic field and investigation of energy characteristics of spectral lines formed near and in the atmosphere of the donor**

From the above it follows that the donor magnetic field significantly influences the overall picture of the localization and formation of developed gaseous structures. A more active region of the outflow of matter from the donor surface is the region of the magnetic pole facing the gainer. A mass-losing donor with the decentered magnetic dipole has a deformed surface, reaching its Roche cavity.

This stimulated a parallel study of the phase variability in the energy characteristics of different lines, which are formed in both the conditions of this peculiar atmosphere and the neighborhood of the donor surface. This applies, above all, to spectral observations made in the red spectral region in 1985-1992 using a CCD detector on the 2.6-m CrAO telescope and, in particular, a comprehensive study of all components of the complex structure of the Si II  $\lambda\lambda$  6347, 6371 lines (Skulskij, 1993b). The phase variability of the equivalent width  $W_\lambda = f(P)$  and  $I_l/I_c = f(P)$ , i.e., the emission intensity ratio in the line to the continuum, in the emission component of Si II  $\lambda\lambda$  6347, 6371 lines shows that there is a well-defined modulation of these Si II emission curves by the donors magnetic field.

The phase dependence of the intensity ratio of the violet to red emission peaks  $I_v/I_r = f(P)$  in the He I  $\lambda$  7065 line (see Fig. 6) was also investigated by Skulskij (1993a). The emission of the He I  $\lambda$  7065 line is interesting because its emission peaks are comparable in intensity, and this is the only line where its violet peak even slightly exceeds the red peak over a considerable phase range close to the 0.35P phase, that is in the range of phase visibility of the donor's magnetic field pole. The minimum ratio of their intensity (i.e., when the red peak dominates) coincides with phases of visibility of the opposite pole of the donor facing the gainer, i.e., of 0.85P. Thus, the dependence of  $I_v/I_r = f(P)$  is also clearly modulated by the spatial structure of the donor's magnetic field. It also means that the emission in both the strong He I  $\lambda$  7065 line and Si II  $\lambda\lambda$  6347, 6371 lines, with their relatively not high emission, is produced largely in some medium in the immediate vicinity of the donor. In addition, Skulskij (1993a) also investigated the phase dependence of the ratio  $\Delta W_\lambda/W_\lambda$ , i.e., of the equivalent width of the absorption component in a range of the total emission to the total emission under the Gaussian profile in  $H_\alpha$  and He I  $\lambda$  7065 lines, which can explain the variability of the self-absorption in this emission. For both lines, this parameter has maxima in phases that coincide with the phases of the two magnetic field poles visibility. In this article, phase variations of the equivalent width of the He I  $\lambda\lambda$  3867, 4120 absorption lines of the donor's atmosphere and the total emission in the He I  $\lambda$  7065 as lines of one helium triplet were also studied. Phase cyclic changes in the equivalent width inherent in the He I  $\lambda\lambda$  3867, 4120 absorption lines of the helium triplet, mainly being synchronized with such  $W_\lambda$ -curve for the He I  $\lambda$  7065 emission line, are found, that is, they have much in common, which is related to the structure of the donor magnetic field.

The investigation of complex Si II  $\lambda\lambda$  6347, 6371 lines also revealed the apparent correlation between the phase variability of the equivalent width of Si II-emissions and such  $W_\lambda$ -curves of absorption lines of this doublet in the donor atmosphere (Skulskij, 1993b). In addition to the effects of the orbital modulation and eclipses, there is a well-defined modulation of these curves by the magnetic field. One also concluded that the formation of emissions in these silicon lines should be localized in the immediate vicinity of the donor surface. This finding

was supported by a new fact: the deep minimum was found on the  $W$ -curves of these Si II emissions in a narrow phase range of 0.02 P duration before the main eclipse of the donor at the phase of 0.96 P in 1991 and 0.93 P in 1992 (Skulskij, 1993b,c). At these phases, the satellite disk, as the outer part of the accretion disk, is projected onto the magnetic pole region on the donor surface facing the gainer, significantly eclipsing the source of the emission in the red Si II doublet (see Figure 1 in Skulskyy (2020)). This can also be interpreted as an eclipse of the hot region of the donor surface or near this surface, i. e., in the direction of the donor magnetic field pole close to the gainer.

The unusual behavior of the equivalent widths of both absorption lines in the red Si II doublet of the donor's atmosphere led to a detailed study of the phase variations of more than 100 absorption lines of this atmosphere in the blue spectral range, published by Skulskij & Vovchik (1971) in the ten main phases of the orbital period. As it turned out, the equivalent widths of the lines of the magnetized and simultaneously outflowing atmosphere of the donor exhibit a special kind of cyclic variations over the orbital period (Skulskij, 1993b). The  $W_\lambda$ -curves of these lines are modulated to varying degrees both by gravitational and magnetic fields. Dozens of the  $W_\lambda$ -curves look like the result of the superposition of harmonic oscillations with different amplitudes and frequencies that are multiples of the orbital frequency. We tried to classify the  $W_\lambda$ -curves in terms of their external form, taking into account the patterns of splitting in the magnetic field and the value of the Lande factors, the total angular momentum of the atoms and the relative intensity of lines in their multiplets, the degree of excitation and ionization. No definite regularities have been discerned, but virtually all absorption lines can be grouped into three types. The first type includes the lines whose  $W_\lambda$ -curves are more definitely subject to orbital modulation. These are more excited or resonance lines, e. g., more intense lines of dominant FeII and TiII multiplets, for which the maxima of their equivalent widths occur, as a rule, at phases around 0.0 P and 0.5 P, i.e., related in space to the line on star-components. It may seem that this group of lines originates in the upper layers of the donor atmosphere, which is extended to its Roche cavity and has a somewhat elongated surface, especially in the gainer direction. The equivalent widths of the second group lines are more clearly correlated with the phase variability of the donor magnetic field, i.e., with the direction of the dipole axis of its magnetic field passing through the 0.35 P and 0.85 P phases. This group includes, as a rule, not very strong absorption lines and lines of a higher degree of excitation and ionization, i.e., lines originating in the relatively deeper layers of the atmosphere. The third, intermediate, group of lines demonstrates the variations in their equivalent widths as a reflection of possible simultaneous actions of the gravitational and magnetic fields.

It is most likely that the demonstrated diagrams of phase variations of the equivalent width and intensity of the different lines of visual spectrum reflect real changes in the physical conditions, both with the depth of the donor atmosphere and above the atmosphere level. However, this occurs both under the

conditions of the specific spacial structure of the donor magnetic field and its deformed surface close to its Roche cavity. This can be seen, for example, from gradual changes in the profiles of lines of the Balmer series. The first members of the series, as shown in the previous sections, are formed above the surface of the donor and further in the moving gaseous structures. They exhibit strong emission components that gradually decrease in intensity and fall under the continuous spectrum close to H7. The high terms of the Balmer series, which are undistorted by emission, according to Figure 6 in Skulskij (1993b), show the notable systematic change of the  $W_\lambda$  -curves from line to line over the orbital period from H9 to H21. In particular, in  $W_\lambda$  -curves of lines H11 - H16 there are here definite narrow local maxima. At the same time, equivalent widths of lines H17 - H20 show here very deep local minima; moreover, during the orbital turning of the donor from the 0.5 P phase to the phase of 0.85 P, the equivalent widths of lines H17 - H19 decreased to one-third of their initial widths. All this going out that the behavior of the spectral lines of the Balmer series, from its high terms up to the  $H_\alpha$  line, reflects a certain change in physical conditions in the donor atmosphere and above its surface. These data also indicate the most pronounced stratification of these conditions in the phase range  $(0.85 \pm 0.15) P$  at the passing of the observer above the donor surface magnetic pole. It could be indicated that similar phase diagrams of variations of the equivalent widths for these hydrogen lines are shown in Bahyl (1986), where there also were noted coordinated phase variations of the equivalent widths for some spectral lines of metals and neutral helium in the donor's atmosphere with phase variations of the donor magnetic field. Hence, this can be seen as a confirmation of our understanding and interpreting mass transfer processes in the Beta Lyrae system based on the concept of the formation of magnetized accretion structures at the presence of a certain spatial configuration of the donor magnetic field.

### 2.5. Magnetic field and the identification of the donor magnetic pole facing the gainer

In view of the above, the next important task was, on the basis of different observations, to attempt to directly identify on the donor surface the range phase visibility of the magnetic pole facing the gainer.

It should draw attention in this regard the accurate infrared photometry of the Beta Lyrae system in 5 bands from J ( $1.2 \mu\text{m}$ ), H ( $1.6 \mu\text{m}$ ), K ( $2.2 \mu\text{m}$ ) to L ( $3.5 \mu\text{m}$ ) and M ( $4.6 \mu\text{m}$ ) that was carried out by Zeilik et al. (1982) in 1977-1982 on the 1.3-m telescope at the Kitt Peak National Observatory. In these observational data, several points that need more attention are apparent. The general shape of these light curves is similar to the visual light curves. The data, collected in Figures 1-5 pursuant to the J, H, K, L, and M filters as for observations in different years (they are demonstrated as magnitude differences of  $(\beta \text{ Lyr} - \alpha \text{ Lyr})$  at statistical errors per point that are typically less than the symbol size), have a good convergence. As expected (according to the previous article of

Jameson & Longmore (1976), where observations were also made using  $\alpha$  Lyrae as a standard star), the depth of the primary eclipse decreases relative to the depth of the secondary eclipse at longer wavelengths and the magnitude differences (in the mag) are such: 0.28 at J, 0.24 at H, 0.12 at K, -0.06 at L, and 0.16 at M bands. Equality of eclipses depths occurs at  $3 \mu\text{m}$ . Previous observations of Jameson & Longmore (1976) also clearly showed a greater secondary eclipses depth in the close bands at  $3.6 \mu\text{m}$ ,  $4.8 \mu\text{m}$ , and especially at  $8.6 \mu\text{m}$  (the last band is absent in Zeilik et al. (1982)). The difference between the maxima on the light curve in the quadratures is particularly noticeable at  $8.6 \mu\text{m}$ , where the asymmetry of the light curve is 0.4 mag, with the maximum of the light curve near the 0.35 P phase, i.e., in the phases visibility of the magnetic pole on the donor surface in the primary quadrature. Jameson & Longmore (1976) noted that at  $3.6 \mu\text{m}$ ,  $4.8 \mu\text{m}$ , and  $8.6 \mu\text{m}$  the infrared light curves have also some fine structure in the phases of the secondary quadrature, which is important in the analysis of the data of Zeilik et al. (1982).

Our review of the observational data in both articles cites that, in the secondary quadrature near the 0.85 P phase, on the four light curves in the range of  $3.5\text{-}4.8 \mu\text{m}$  one can see clear local segments of the radiation increase. They permit in this phase the direct identification on the donor surface of the magnetic field pole region close to the gainer. This draws up primarily from the more accurate M band data in Fig. 7, which is introduced as Figure 5 from the article of Zeilik et al. (1982). This light curve has the secondary eclipse depth of -2.92 mag in phase 0.5 P and, reaching a value of -2.6 mag in phase 0.68 P, remains practically invariable until phase 0.80 P. From phase 0.81 P the light curve increases abruptly by 0.20 mag to phase 0.85 P, reaching here the maximum value near of -2.4 mag, and then decreases to the previous value of -2.6 mag in phase near 0.90 P and to -3.08 mag in phase 0.0 P of the primary eclipse. According to Table 1 and Figure 1 of Jameson & Longmore (1976), the light curve at the band of  $4.8 \mu\text{m}$  for averaged observations in the 0.81 P and 0.88 P phases also show the identical increase of 0.2 mag, respectively, from -2.65 mag to -2.45 mag, followed by a rapid drop on the light curve to the 0.95 P phase (these observations were not performed often enough). As one can see from Fig. 7, a sharp and clear radiation increase in the light curve at the M band demonstrates the effective phase width of visibility of this hot region close to 0.1 P. The maximum in this light curve coincides with the maximum of the magnetic field curve at the 0.855 P phase (Burnashev & Skulskij, 1991), which corresponds to the phase of the meridional passage of the magnetic pole on the donor surface (see also Fig. 1).

Hence, the light curves at M band ( $4.6 \mu\text{m}$ ) from Zeilik et al. (1982) and at the band of  $4.8 \mu\text{m}$  from Jameson & Longmore (1976) can be quite convincing evidence of the spatial identification on the donor surface of the magnetic field pole facing the gainer. The result of this kind is understandable because at these wavelengths the optical depths are smaller, and this allows one to see the radiating matter above the donor surface deeper, where the effective temperatures

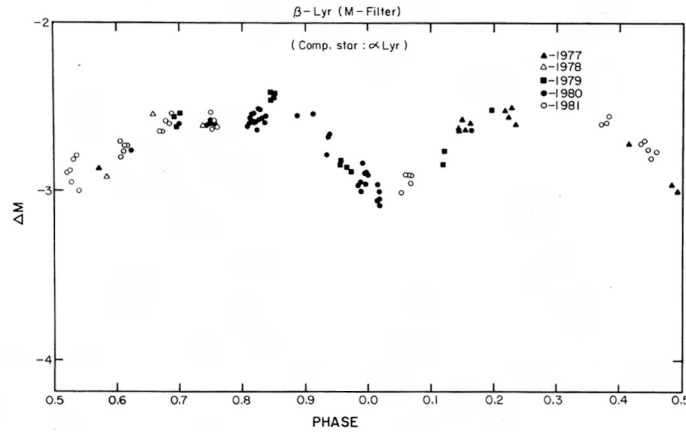


**Figure 7.** Raw data as magnitude differences ( $\beta$  Lyr -  $\alpha$  Lyr) for  $\beta$  Lyr at M band ( $4.6\mu\text{m}$ ). Dates are, 1977 (closed triangles), 1978 (open triangles), 1979 (closed square), 1980 (closed circle) and 1981 (open circle). Statistical errors per point are typically less than the symbol size (Zeilik et al., 1982).

are higher. This identification is confirmed from the point of view measuring the Zeeman splittings in the Si II  $\lambda\lambda$  6347, 6371 lines according to observations with the CCD detector on the 2.6-m CrAO telescope (Skulskij & Plachinda, 1993). The obtained curve of effective magnetic field strength in the Si II lines changes with the orbital phase synchronously with the photographic curve of the magnetic field shown in Fig. 1. However, on these curves in Si II lines there are two regions in which one sees the locally changing polarity of the magnetic field with a width of approximately 0.08 P (see Figures 5 and 6 in Skulskij (2020)). Their centers are located exactly in the phases 0.355 P and 0.855 P of both poles of the magnetic field on the donor surface. This coincidence can be considered as the independent identification of the magnetic poles on the donor surface. On the other hand, the hot region on the donor surface in the phases around the pole of the magnetic field facing the donor was confirmed by the independent researches of the spectrum near the Si II  $\lambda\lambda$  6347, 6371 lines by Skulskij (1993b,c). First, this region on the donor surface is identified as the clear-cut of its deep eclipse when the satellite disk, as the outer part of the accretion disk, is passing above the donor surface (see Figure 4b in Skulskij (1993c)). Second, these CCD observations of 1991 and 1992 showed that the phase variations of both the equivalent widths of these absorption lines of the donor atmosphere and the emission component of these lines practically identically reflect the phase variations of the donor the magnetic field, confirming that the regions of formation of all these lines are close to each other.

One can summarize those methodically independent observations and in-

vestigations of Zeilik et al. (1982); Jameson & Longmore (1976); Skulskij & Plachinda (1993), and Skulskij (1993b,c). They admit evidence of the phase boundaries of orbital identification of the magnetic pole facing the gainer on the donor surface and argue that the emissions of the Si II  $\lambda\lambda$  6347, 6371 lines are generated actually fairly close to the donor surface, mainly around the location region of this magnetic pole. Moreover, it should be supposed that a hot region centered at the phase of 0.80 P, which was interpreted in Mennickent & Djurašević (2013) as detected on the accretion disk (see Figure 1 in Skulskyy (2020)), may, in fact, be caused by additional radiation in these phases directly from the magnetic-polar region on the donor surface. This is one of the consequences of the spatial identification on the donor surface the magnetic pole facing the gainer.

It is now pertinent to note that the identification at the donor surface of additional radiation in the magnetic pole region, as well as of the phase boundaries of this radiation, is important for understanding the nature of the developed gaseous structures in the Beta Lyrae system. In this binary system, as in helium stars with the magnetically controlled matter, magnetized plasma can be directed outwards, forming matter outflows from the magnetic polar region. Indeed, Shore & Brown (1990) proposed a known model for helium stars, the essence of which is that “circumstellar plasma is trapped in the stellar magnetosphere near the magnetic equator or is channeled to form jetlike outflows from the magnetic polar regions”. With regard to the first statement, it is worth mentioning the phenomenon of depression at  $\lambda$  5200 Å in the continuum of the Beta Lyrae system, which was discovered and studied as an independent argument for the reality of the magnetic field (Burnashev & Skulskij, 1986). Both maxima of the equivalent width of this depression are observed in the same phases as the zones of both poles of the magnetic field on the donor surface. At the same time, both minima of the equivalent width of this depression are clearly displaced by a quarter of the orbital period, indicating that the direction perpendicular to the axis of the magnetic field may be important.

The model of Shore & Brown (1990) is based on the observed correlations between the line profiles characteristics of the C IV and Si IV ultraviolet resonance doublet, the variations in the strength of these lines, and the inferred magnetic field geometry in helium stars (incidentally, the atmosphere of the donor also has excess helium). In Fig. 8 (representing Figure 11b of Shore and Brown (1990)) depicts the model of a helium star as an oblique magnetic rotator. This model may be to some extent illustrative of the donor as an oblique magnetic rotator since the dipole axis of its magnetic field is deviated by  $28^\circ$  relative to the orbital plane of the binary system (Skulskij, 1985). Given that the center of the magnetic field dipole of the donor is substantially displaced in the direction of the gainer, additional outflows of matter from the donor surface in the direction of the magnetic axis of the donor may show an unusual, but the predictable picture of the mass transfer. This picture, although complicated by real magnetohydrodynamics, must be reflected in some way in both the accre-

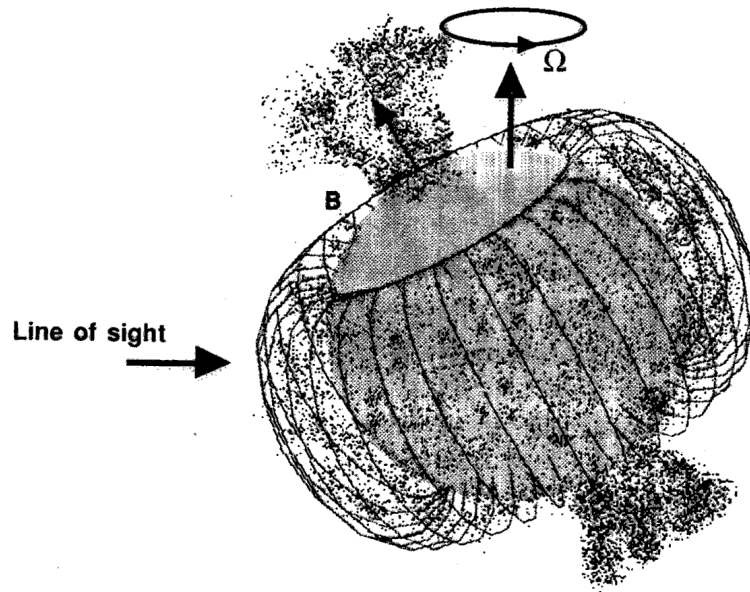


**Figure 8.** A cartoon illustrating the geometry of the proposed model for an oblique rotator of intermediate obliquity (Shore & Brown, 1990)

tionary structures between the components (that is investigated in this article) and the circumbinary structures surrounding the Beta Lyrae system (it is a task of the next article).

### 3. Conclusions and discussion

Throughout the present investigation, it has been confirmed that two types of magnetic field studies by Skulskij (1985, 1990), based on observations of the 6-m SAO telescope; and Skulskij & Plachinda (1993) based on CCD observations of the 2.6-m CrAO telescope), show reasonable expectations in the certain phase correlation with each other. Although their averaged absolute values are different, their phase curves of the magnetic field are similar on the whole: they capture the direction of the magnetic field dipole and phases of visibility of the two poles on the donor surface. This made it possible to more reliably study various physical processes reflected in their phase variability parallel with the corresponding variability of the donor magnetic field. In Skulsky (2020) it is shown that a quasi-sinusoidal photographic curve of the magnetic field, which is similar to such curves of magnetic stars, is more appropriate for this type of research. In the previous sections this approach is worked out on the basis of a number of obvious facts obtained from the analysis of various spectral

and spectrophotometric observations mainly in the visible spectrum of this binary system. The focus was on the existence of correlations between the orbital variability of the magnetic field and the analogous variability of certain parameters in different physical processes, primarily due to studying the dynamic and energy characteristics of complex emission-absorption lines. First of all, the variable structure of gas flows in the processes of accretion and mass transfer between components of the binary system and the reflection of such magnetized spatial structures in the orbital variability of the magnetic field was studied. The following are some of the key points of this study as a certain phenomenon.

No doubt, the important result was the obtaining of the curve of the phase variability of the absolute radiation flux in the  $H_\alpha$  emission line as a certain fact in its evident interconnection with the phase variability of the magnetic field of the donor (see Fig. 1 in section 2.1). Firstly, the curve of the variability of the absolute radiation flux in the  $H_\alpha$  line clearly displays the direction of (0.355-0.855) P of the donor magnetic field maxima and its dipole axis. Secondly, between the extrema of the magnetic field, the radiation flux in the  $H_\alpha$  line increases 1.3 times: this flux has a minimum level in the phases near 0.355 P of the first quadrature, i.e., in phases of the observation of the magnetic field pole on the donor surface, and the maximum level in phases of the second quadrature round the 0.855 P phase, i.e., in phases of the observation on the donor surface of the magnetic field pole facing the gainer. Thirdly, the apparent additional radiation flux in the  $H_\alpha$  line determines the center and the phase limits ( $0.43 \pm 0.06$ ) P of the known hot region of radiating medium projected onto the accretion disk. It is most certain that the effect obtained is the result of a direct collision of gaseous flows with the accretion disk. All in all, one can conclude that the magnetic field is directly reflected in the radiating accretion structures formed during the matter transfer in the Beta Lyrae system.

The above-giving finding is supported by the high-speed variability of the Beta Lyrae spectrum in the region of the  $H_\alpha$  line (see section 2.2). An unusually broad base emission component, with a total width of more than 6000 km/s under a known emission peak with a total width of up to 700 km/s, was detected. This broad emission has the highest continuum in the phases of two quadratures and near phases of the donor magnetic field poles. Such spread wings of the broad emission indicate high speeds of the radiating atoms and reflect directions of the observation of the more high-temperature hydrogen medium. Simultaneously, in these phases, there is the most chaotic variability in the shape and the intensity of the entire emission on 10-second spectra, in both the central peak of the  $H_\alpha$  emission line and its broad emission component. In vision phases of the magnetic field pole facing the gainer, concretely at phase 0.81 P, there was recorded an event of the eruptive nature, which is formed by two components: “emission flare-up” and “traveling absorption”. This may reflect a high-velocity matter outflow or even gas jets from a binary system but, that is important, this event took place in the neighborhood of the donor magnetic field pole. Indeed, the characteristic time of the event indicates the local spatial

and temporal characteristics of the movement of gaseous structures close to the donor surface.

This conclusion is supported by other energetics parameters. The phase dependence of the intensity ratio of the violet and red emission peaks of  $I_v/I_r = f(P)$  in the He I  $\lambda$  7065 emission line reflects two extrema on the curve of the effective magnetic field at the phases 0.355 P and 0.855 P, which correspond to the visibility phases of the donor magnetic poles (see Fig. 6b). This is the only emission line of the visual spectrum in which its violet peak exceeds the red peak in the 0.355 P phase, indicating additional radiation directed at the observer. The red peak, as in the  $H_\alpha$  emission line, dominates in the 0.855 P phase, i.e., in the phase of the visibility of the opposite donor magnetic pole facing the gainer. Hence, the dependence of  $I_v/I_r = f(P)$ , which reflects the radiation gas structures near the donor, is modulated by the spatial configuration of the donor's magnetic field. The study of the intensity and equivalent width of the various lines formed in both the conditions of the donor peculiar atmosphere reaching its Roche cavity and the immediate vicinity of the donor (2.4) shows that the donor magnetic field significantly influences their behavior. For example, a clear correlation was found between the phase variations of the equivalent width of Si II-emissions and such dependence  $W_\lambda = f(P)$  for absorption lines of these complex Si II  $\lambda\lambda$  6347, 6371 lines in the donor's atmosphere. There is an apparent modulation of these curves by the donor magnetic field. This also can be seen from gradual changes in the profiles of lines of the Balmer series from their first to the highest members of the series. The most clearly pronounced stratification in physical conditions in the donor atmosphere and above its surface is observed in the phases of  $(0.85 \pm 0.15)P$ , i.e., in phases of the visibility of the donor magnetic pole facing the gainer. Thus, the aforementioned and other factors indicate this important phase region of the matter loss from the deformed donor surface. However, only the analysis of the light curves at M band ( $4.6 \mu\text{m}$ ) and others (see section 2.5) allowed the direct identification on the donor surface of the magnetic pole facing the gainer. The effective width of its phase visibility is near 0.1 P and its center matches the 0.855P phase of the magnetic pole center.

Parallel with the above energetics parameters, the correlation ligaments of the effective magnetic field strength of the donor in its variability over the orbital phases with the dynamics characteristics of the  $H_\alpha$  emission line and other known lines of visual spectrum are equally compelling. Three variable structural components are traditionally measured: two emission peaks and the absorption feature between these emission peaks. The measurement of the Doppler shifts of the components of these emission lines showed that the new parameter we introduced (Skulskij & Malkov, 1992), namely the Gaussian emission center as a whole, became the most informational. Subsequent observations and reliable measurements of the high-resolution CCD spectra (Skulskij, 1993a) confirmed that the radial velocity curves of such centers of emission profiles (primarily  $H_\alpha$  and He I  $\lambda$  7065) fully correspond to the orbital curve of the magnetic donor

field variability (see section 2.3). Indeed, the radial velocity of the center of this total emission (see Fig. 5 and 6) shows that both maxima clearly match the two extrema of the sinusoidal curve of the effective magnetic field strength of the donor (see Fig. 1). This indicates that these two curves reflect physically related phenomena. It should be supposed that the emission as a whole of complex emission-absorption lines is essentially formed under the influence of the spatial structure of the donor magnetic field, which is reflecting by the (0.355-0.855) P phases of its dipole axis. Moreover, the dynamical characteristics of the Gaussian profile of  $H_\alpha$  emission as a whole fully match the findings of the orbital variability of the absolute radiation flux in the  $H_\alpha$  emission line (see the above and section 2.1), i.e., the dynamic and energy characteristics of this emission are formed to a large extent in magnetized structures near the donor. This is an important conclusion.

The second important finding follows also from measuring these Doppler shifts: the absorption feature in the limits of the total double-peaked emission is the result of self-absorption in magnetized structures surrounding the donor. This result became better clear after comparing the radial velocity curves of the absorption cores of all the studied complex lines, primarily  $H_\alpha$  and He I  $\lambda$  7065. This can be seen in Fig. 6c, where the absorption component of the He I  $\lambda$  7065 line reaches positive velocities of +15 km/s in phases (0.35-0.55) P (that is, the movement of absorption material flowing off from the donor surface in the direction from the observer), while for the  $H_\alpha$  line and the rest of the lines this component has a known minimum of -15 km/s in the phase of the accretion disk eclipse by the donor (the motion of this matter to the observer). It means that dynamic parameters of the radiating and absorption medium, in which these lines are formed, differ in both density and excitation conditions; i.e., such medium is substantially stratified.

There are some other points as to dynamics and the spatial formation of the radiating-absorption gaseous structures. Figure 6c demonstrates that the absorption components of all the studied lines reach a known maximum negative radial velocity of -115 km/s (close to parabolic) in the direction of the gainer in phases of about 0.05 P. This can be explained by the action of Coriolis force that form the main gas flow within the Roche cavity of the gainer. Such flow does not leave the limits of the gainer gravity and is important for the formation of an accretion disk around the gainer (see Skulskyy (2020)). It is important to note again the direction of motion of the radiating plasma along the donor axis. Figure 6c shows that positive radial velocities of +15 km/s of the absorption component on the He I  $\lambda$  7065 emission line, closely 0.355 P phases of the observation of the donor magnetic pole, reflect, in fact, the direction of the mass loss from the donor surface toward the opposite donor magnetic pole facing the gainer. From Fig. 5d it is well discernible that the violet peak of all the studied lines reaches the maximum value of the negative radial velocity of -200 km/s (to the observer) in the phase of 0.855 P of the observation of the donor magnetic pole facing the gainer. Besides, the radial velocity curve for the more intense

red emission peak in Fig. 5a has two maxima of the positive radial velocity at phases of the observation of both donor magnetic poles. In general, all this can be interpreted as the matter outflow from the region of the magnetic poles of the donor surface along the direction of (0.355-0.855) P of the magnetic field axis. In the process of the formation of moving accretionary structures, the decisive role is played by the donor magnetic pole facing the gainer.

Thus, the above-giving specification of the main results, presented in the form of some research discussion, suggests the concept of formation of developed spatial accretion structures in the Beta Lyrae system in the presence of the donor magnetic field. It can be summarized as follows.

The analysis of a number of spectral and spectrophotometric observations showed that the structure of the gaseous flows between the donor and the gainer is largely due to the specific dipole configuration of the donor magnetic field. The axis of the donor magnetic field, which reflects the two extrema of the magnetic field strength curve, there is in the direction in the orbital phases of (0.355-0.855) P and is deflected from the phases axis of (0.5-1.0) P, i.e., from the direction of the gravitational axis of the stellar components. The magnetic field axis is inclined to the orbital plane by an angle of  $28^\circ$ . The center of the donor magnetic dipole is displaced by 0.08 of the distance between the centers of gravity of both components toward the gainer center. The magnetic pole, which is observed in the phases near 0.855 P, is located on the donor surface slightly above the orbital plane and closer to the gainer. The localization of this magnetic pole is important in the context of a few next issues. The ionized gas channeled by the donor magnetic field moves in the direction of its dipole axis from the donor surface and deflects along the magnetic field lines toward the accretion disk. In the space between the donor and the gainer during the matter motion, there is formed a system of developed magnetized radiating flows, which is clearly reflected from the study of their physical characteristics, especially in the second quadrature. Effective shock collisions of the magnetized plasma in the phases of this second quadrature of (0.6-0.8) P are enhanced by the rapid counter-rotation of the accretion disk with the formation of a high-temperature medium and a hot arc on its outer rim facing the donor. In the plane with the axis of the magnetic field, there is a significant vertical component of the flux of the magnetic induction vector, which can be responsible for the gaseous jets observed as perpendicular to the plane of the orbit.

It should be noted that the obtained picture characterizes, first of all, the accretion structures in the space between the two stellar components. A more general picture must be created from the study of expanding structures surrounding this binary system. Some points of such study are published in Skulsky (2015). More thorough research is planned to be published in the next article.

**Acknowledgements.** The author is thankful to Kudak V.I. for consultations.

## References

- Alexeev, G. N. & Skulskij, M. Y., Rapid variability of the spectrum of  $\beta$  Lyrae in the  $H_{\alpha}$  region. 1989, *Bull. Spec. Astroph. Obs.*, **28**, 21
- Appenzeller, I. & Hiltner, W. A., True Polarization Curves for Beta Lyrae. 1967, *Astrophys. J.*, **149**, 353, DOI: 10.1086/149258
- Aydin, C., Brandi, E., Engin, S., et al., A study of the continuum flux and the line structure in the IUE spectrum of  $\beta$  Lyrae. 1988, *Astron. Astrophys.*, **193**, 202
- Bahyl, V., Equivalent Widths of the Spectral Lines of the  $\beta$  Lyrae System and Their Changes. 1986, *Bull. Astron. Inst. Czechosl.*, **37**, 42
- Batten, A. H. & Sahade, J., The Emission Profile of  $H_{\alpha}$  in the Spectrum of  $\beta$  Lyrae. 1973, *Publ. Astron. Soc. Pac.*, **85**, 599, DOI: 10.1086/129511
- Bisikalo, D. V., Harmanec, P., Boyarchuk, A. A., Kuznetsov, O. A., & Hadrava, P., Circumstellar structures in the eclipsing binary eta Lyr A. Gasdynamical modelling confronted with observations. 2000, *Astron. Astrophys.*, **353**, 1009
- Bless, R. C., Eaton, J. A., & Meade, M. R., Random variations in the ultraviolet spectrum of  $\beta$  Lyrae. 1976, *Publ. Astron. Soc. Pac.*, **88**, 899, DOI: 10.1086/130043
- Burnashev, V. I. & Skulskij, M. Y., Variability of the 5200 Å in  $\beta$  Lyrae and  $\nu$  Sagittarii. 1986, *Pisma v Astronomicheskii Zhurnal*, **12**, 535
- Burnashev, V. I. & Skulskij, M. Y.,  $H_{\alpha}$  photometry and magnetic field of  $\beta$  lyrae. 1991, *Izv. Krymskoj Astrofiz. Obs.*, **83**, 108
- Harmanec, P., Morand, F., Bonneau, D., et al., Jet-like structures in  $\beta$  Lyrae. Results of optical interferometry, spectroscopy and photometry. 1996, *Astron. Astrophys.*, **312**, 879
- Hoffman, J. L., Nordsieck, K. H., & Fox, G. K., Spectropolarimetric Evidence for a Bipolar Flow in beta Lyrae. 1998, *Astron. J.*, **115**, 1576, DOI: 10.1086/300274
- Ignace, R., Gray, S. K., Magno, M. A., Henson, G. D., & Massa, D., A Study of  $H_{\alpha}$  Line Profile Variations in  $\beta$  Lyr. 2018, *Astron. J.*, **156**, 97, DOI: 10.3847/1538-3881/aad339
- Jameson, R. F. & Longmore, A. J., Infrared observations and a model for  $\beta$  Lyr. 1976, *Mon. Not. R. Astron. Soc.*, **174**, 217, DOI: 10.1093/mnras/174.1.217
- Kondo, Y., McCluskey, G. E., Silvis, J. M. S., et al., Ultraviolet Light Curves of beta Lyrae: Comparison of OAO A-2, IUE, and Voyager Observations. 1994, *Astrophys. J.*, **421**, 787, DOI: 10.1086/173691
- Lomax, J. R., Hoffman, J. L., Elias, Nicholas M., I., Bastien, F. A., & Holenstein, B. D., Geometrical Constraints on the Hot Spot in Beta Lyrae. 2012, *Astrophys. J.*, **750**, 59, DOI: 10.1088/0004-637X/750/1/59
- Mennickent, R. E. & Djurašević, G., On the accretion disc and evolutionary stage of  $\beta$  Lyrae. 2013, *Mon. Not. R. Astron. Soc.*, **432**, 799, DOI: 10.1093/mnras/stt515
- Sahade, J., Huang, S. S., Struve, O., & Zeberg, V., The Spectrum of Beta Lyrae. 1959, *Transactions of the American Philosophical Society*, **49**, 1

- Shore, S. N. & Brown, D. N., Magnetically Controlled Circumstellar Matter in the Helium-strong Stars. 1990, *Astrophys. J.*, **365**, 665, DOI: 10.1086/169520
- Skulskij, M. Y., Quantitative analysis of  $\beta$  Lyrae spectra. I. Variations of some hydrogen and helium lines. 1972, *Izv. Krymskoj Astrofiz. Obs.*, **45**, 135
- Skulskij, M. Y., Short-term fluctuations of hydrogen and helium emission in the spectrum of  $\beta$  Lyrae. 1980, *Pisma v Astronomicheskii Zhurnal*, **6**, 628
- Skulskij, M. Y., Beta Lyrae as a magnetic binary star. 1982, *Sov. Astron. Lett.*, **8**, 126
- Skulskij, M. Y., The Magnetic Field of the Beta-Lyrae System. 1985, *Sov. Astron. Lett.*, **11**, 21
- Skulskij, M. Y., The magnetic field and tidal resonant phenomena in  $\beta$  Lyrae. 1990, *Mitteilungen KSO Tautenberg*, **125**, 146
- Skulskij, M. Y., Study of  $\beta$  Lyrae CCD spectra. Absorption lines, orbital elements and disk structure of the gainer. 1992, *Sov. Astron. Lett.*, **18**, 287
- Skulskij, M. Y., Spectra of  $\beta$  Lyr. Matter transfer and circumstellar structures in presence of the donors magnetic field. 1993a, *Astron. Lett.*, **19**, 45
- Skulskij, M. Y., Spectra of  $\beta$  Lyr the SiII  $\lambda\lambda$  6347, 6371 doublet and the cyclic variation of the equivalent widths of lines in the "magnetized" atmosphere of the loser. 1993b, *Astron. Lett.*, **19**, 19
- Skulskij, M. Y., The spectrum of  $\beta$  Lyrae: the SiII  $\lambda\lambda$  6347, 6371 doublet in 1992 and its variation from season to season. 1993c, *Astron. Lett.*, **19**, 160
- Skulskij, M. Y. & Malkov, Y. F., Investigation of  $\beta$  Lyrae based on high-dispersion CCD spectrograms near the H $\alpha$  line. 1992, *Soviet Ast.*, **36**, 147
- Skulskij, M. Y. & Plachinda, S. I., A study of the magnetic field of the bright component of  $\beta$  Lyr in the SiII  $\lambda\lambda$  6347, 6371 lines. 1993, *Pisma Astron. Zh.*, **19**, 517
- Skulskij, M. Y. & Vovchik, E. B., The equivalent widths of the absorption lines in the spectrum of beta Lyrae. 1971, *Tsirk. Astron. Obs. Lviv*, **45**, 25
- Skulsky, M. Y., On the nature of the interacting  $\beta$  Lyrae system: location of hot region on accretion disk as representation of the magnetized gas structures. 2015, *Science and Education a New Dimension. Natural and Technical Sciences*, **III(6)**, 6
- Skulsky, M. Y., On the structure of magnetized accretion flows in the system of Beta Lyrae. 2018, *Contrib. Astron. Obs. Skalnaté Pleso*, **48**, 300
- Skulskyy, M. Y., Formation of magnetized spatial structures in the Beta Lyrae system. I. Observation as a research background of this phenomenon. 2020, *Contrib. Astron. Obs. Skalnaté Pleso*, **50**, 681
- Zeilik, M., Heckert, P., Henson, G., & Smith, P., Infrared photometry of beta Lyrae: 1977-1982. 1982, *Astron. J.*, **87**, 1304, DOI: 10.1086/113217

# Exact solution for the rotating polytropes with index unity, its approximations and some applications

M.V. Vavruk and D.V. Dzikovskyi

*Department of Astrophysics, Ivan Franko National University, Kyrylo & Methodiy str. 8, 79005 Lviv, Ukraine, (E-mail: mvavruk@gmail.com)*

Received: July 9, 2020; Accepted: October 11, 2020

**Abstract.** The fundamental stages of development of the polytropic theory of stars with axial rotation are considered as a generalization of the Lane-Emden theory. The solution of the differential equilibrium equation for the polytropic star model with index  $n = 1$  and axial rotation with the angular velocity  $\omega$  is presented in the form of infinite series of the Legendre polynomials and the spherical Bessel functions. Two variants of the approximate solution in the form of the finite number of terms are proposed. Integration constants were found in a self-consistent way using the integral form of the equilibrium equation and the iteration numerical method. Dependence of the geometrical and physical characteristics of the model on the dimensionless angular velocity  $\Omega = \omega(2\pi G\rho_c)^{-1/2}$  (where  $\rho_c$  is the density in the centre) is analyzed. A comparison with the results of other authors is performed. The obtained critical value of the angular velocity  $\Omega_{\max}$ , when an instability occurs is smaller than in other works (Chandrasekhar, 1933; James, 1964, and et al.). The inverse problem is also considered – a determination of the polytropic model parameters for individual stars based on the solution of the equilibrium equation according to the values of their masses and radii, which are known from observations. In particular, the model parameters for the star  $\alpha$  Eri, as well as a similar “class” of the star models of types O5÷G0, were determined. The solution of the equilibrium equation for the polytrope  $n = 1 + \delta$  (where  $\delta$  is a small value) is obtained using the method of perturbation theory.

**Key words:** stars: rotation – stars: interiors – stars: fundamental parameters – stars: statistics – PACS number(s): 97.20.-w

## 1. Introduction

The principles of the polytropic theory of solar-like stars were created by the works of Lane (1870), Emden (1907), Fowler (1930), Eddington (1926) and other researchers in the first half of the last century. This theory is based on the equilibrium equation of a star with the polytropic equation of state

$$P(\mathbf{r}) = K\rho^{1+1/n}(\mathbf{r}), \quad (1)$$

where  $P(\mathbf{r})$  is the pressure at the radius-vector  $\mathbf{r}$ ,  $\rho(\mathbf{r})$  is the local density of matter, and  $K$  and  $n$  are constants. It yields a determination of main relations between the polytrope characteristics and describes stability of stars. An idea of the polytropic dependence between the pressure and density is successfully used for a construction of the cold degenerate dwarfs theory (Chandrasekhar, 1931).

The axial rotation is a factor that is common for various celestial objects – the stars of main sequence, pulsars, white dwarfs and black holes. The equilibrium equation of polytrope without rotation with spherical symmetry of matter distribution is an ordinary differential equation of the second order, which is known as the Lane-Emden-Fowler equation. The equilibrium equation for the polytropic model with axial rotation in a general case (for an arbitrary value of the index  $n$ ) is a non-linear differential equation of second order in partial derivatives. The exact solution of the equation is known only for the particular case  $n = 0$ , from which the Maclaurin formula is obtained (see Chandrasekhar, 1969) that determines the relations between the angular velocity and eccentricity of a rotating homogeneous ellipsoid.

To evaluate the influence of rotation on the Sun's characteristics, Milne (1923) found an approximate solution of the equilibrium equation for  $n = 3$  for the case of a small angular velocity, by linearizing the equation. Such approximation corresponds to the first order of perturbation theory. Using the method of Milne (1923), Chandrasekhar (1933) obtained the solutions with the help of a numerical integration for the polytropes with indices  $n = 1.0, 1.5, 2.0, 2.5, 3.0$ . Kopal (1937) pointed out that in the particular case of  $n = 1$  with an axial symmetry the equilibrium equation allows for a separation of variables. He found a set of fundamental solutions in the form of products of the Legendre polynomials and the spherical Bessel function of the first kind. However, the question of finding a general solution, by the given boundary conditions, Kopal did not consider.

James (1964) went beyond a small rotational velocity approximation. He found an approximate solution for the polytropes with indices  $n = 1.0, 1.5, 2.0, 2.5, 3.0$  and calculated dependence of the polytrope characteristics on the angular velocity in the interval  $0 \leq \omega \leq \omega_{max}(n)$ . Unfortunately, the solutions were not presented in the publication, which makes it impossible to analyze their dependence on the angular velocity as well as to use the solutions for the calculation of other characteristics.

In the work of Monaghan & Roxburgh (1965) there is generalized the Milne – Chandrasekhar approach by a more accurate description of the outer polytrope region. Aiming to find integration constants (Milne, 1923; Chandrasekhar, 1933) and also to determine the fitting parameters (Monaghan & Roxburgh, 1965), the authors applied the traditional in the stellar surface theory approximation, which is based on the usage of the general multipole form of potential, created by an unknown distribution of matter in the inner part of the star. The common characteristic of these works is the first approximation relative to ro-

tation influence. Therefore integration constants and fitting parameters do not depend on the angular velocity, but only on the polytropic index (Milne, 1923; Chandrasekhar, 1933; Monaghan & Roxburgh, 1965). The partial solution of the equilibrium equation which is considered by Caimmi (1980) at  $n = 1$ , improves Chandrasekhar's solution (Chandrasekhar, 1933) by the determination of integration constants numerically.

In spite of the long research history, the problem of the calculation of characteristics of the polytropic model remains relevant and has both methodological and applied importance. It should be mentioned recent works of Kong et al. (2015) and Knopik et al. (2017), in which the computer methods were used to calculate the characteristics of individual stars based on the polytropic model at  $n = 1$ . The polytrope model is a good zero approximation for the calculation of the characteristics of massive dwarfs (James, 1964; Vavruk et al., 2010). It can be used to describe neutron stars, circumstellar disks, gas giant planets, and in the theory of stability and pulsation of stars.

In the work of Vavruk et al. (2019) it is shown that the finding of the solutions of the equilibrium equation for the polytropes with rotation more accurately requires the usage of a multi-component expansion for the Legendre polynomials. In this case the correct definition of integration constants is provided by the integral form of the equilibrium equation, which is equivalent to the explicit calculation of gravitational potential at some point of polytrope by the known solution of the equilibrium equation.

The model with  $n = 1$  plays the role of the standard in the polytropic theory. Finding a solution of a linear inhomogeneous differential equation of the second order with partial derivatives is a simpler problem than finding solutions of a non-linear equation at  $n > 1$ . Therefore, with polytrope with  $n = 1$  there is tested a new method of finding the equilibrium equation solutions, which can be generalized later for the model with an arbitrary  $n$ . The problem of calculation of the polytropic characteristics with  $n = 1$  has independent meaning, as an example of the problem that allows for solutions with high precision. The maximal value of the angular velocity for this model is quite large ( $\Omega_{\max} = 0.245$ ), therefore it is suitable for the calculation of the characteristics of the individual observed stars with rapid axial rotation.

The purpose of our work is to obtain the correct analytical approximation of the solution of the equilibrium equation for the polytrope with  $n = 1$  and solid-body rotation. In this way we simultaneously use differential and integral forms of the equilibrium equation (section 2). Two representations of the solution of the differential equation in the form of the infinite series, as well as two basic approximations in the form of the finite number of terms, are shown in section 3. The self-consistent method of the calculations of integration constants based on the integral equation is described in section 4. The results of calculations of the polytrope characteristics dependence and integration constants on the angular velocity are shown in section 5. In section 6 it is shown the way how the solution of the equilibrium equation of the polytrope with  $n = 1$  can be used to find an

approximate solution at  $n = 1 + \delta$ , where  $\delta$  is a small value. The application of the found basic approximations and their linear combinations is considered in section 7, where the polytropic model is built for the star  $\alpha$  Eri and models for the stars of classes O5–G0.

## 2. The two forms of the equilibrium equation

In the presence of rotation the hydrostatic equilibrium equation is rewritten in the non-inertial (rotating) coordinate system in the form (Chandrasekhar, 1933)

$$\nabla P(\mathbf{r}) = -\rho(\mathbf{r}) \{ \nabla \Phi_{\text{grav}}(\mathbf{r}) + \nabla \Phi_c(\mathbf{r}) \}, \quad (2)$$

where

$$\Phi_{\text{grav}}(\mathbf{r}) = -G \int \frac{d\mathbf{r}' \rho(\mathbf{r}')}{|\mathbf{r} - \mathbf{r}'|} \quad (3)$$

is the gravitational potential inside the star and  $\Phi_c(\mathbf{r})$  is the centrifugal potential. If the axis  $Oz$  of the spherical coordinate system coincides with the axis of rotation, then

$$\Phi_c(\mathbf{r}) = -\frac{1}{2} \omega^2 r^2 \sin^2 \theta. \quad (4)$$

Here  $\theta$  is the polar angle and  $\omega$  is the angular velocity of reference frame, which is considered as constant.

Substituting the expressions (1) for  $n = 1$ , (3) and (4) in Eq. (2) and taking the divergence, the equilibrium equation is obtained in the form of the differential equation that determines the density distribution,

$$2K \Delta \rho(\mathbf{r}) = -4\pi G \rho(\mathbf{r}) + \frac{1}{2} \omega^2 \Delta (r^2 \sin^2 \theta). \quad (5)$$

In the presence of axial symmetry ( $\rho(\mathbf{r}) = \rho(r, \theta)$ ) the Laplace operator is written in the form

$$\begin{aligned} \Delta &= \Delta_r + \frac{1}{r^2} \Delta_\theta, \quad \Delta_r = \frac{1}{r^2} \frac{\partial}{\partial r} \left( r^2 \frac{\partial}{\partial r} \right), \\ \Delta_\theta &= \frac{\partial}{\partial t} (1 - t^2) \frac{\partial}{\partial t}, \end{aligned} \quad (6)$$

at  $t = \cos \theta$ , therefore  $\Delta (r^2 \sin^2 \theta) = 4$ . Introducing the dimensionless radial coordinate  $\xi = r/\lambda$ , as well as using the substitution

$$\rho(r, \theta) = \rho_c Y(\xi, \theta), \quad (7)$$

where  $\rho_c$  is the density of matter in the stellar centre, we transform Eq. (5) to the dimensionless form

$$\Delta_{\xi, \theta} Y(\xi, \theta) = \Omega^2 - Y(\xi, \theta). \quad (8)$$

Herewith the scale  $\lambda_n$ , the dimensionless angular velocity  $\Omega$  and the Laplacian operator are determined by the relations

$$\lambda = \left( \frac{K}{2\pi G} \right)^{1/2}, \quad \Omega = \frac{\omega}{(2\pi G \rho_c)^{1/2}}, \quad (9)$$

$$\Delta_{\xi, \theta} = \Delta_{\xi} + \frac{1}{\xi^2} \Delta_{\theta}, \quad \Delta_{\xi} = \frac{1}{\xi^2} \frac{\partial}{\partial \xi} \left( \xi^2 \frac{\partial}{\partial \xi} \right).$$

According to definition (7),  $Y(0, \theta) = 1$  and the condition  $\partial Y(\xi, \theta)/\partial \xi = 0$  at  $\xi = 0$  corresponds to the solutions regular in the vicinity of  $\xi = 0$ . At large values of  $\Omega$  the non-monotonous dependence  $Y(\xi, \theta)$  on the variable  $\xi$  in the equator region, as well as the leakage of matter, are possible. The stability conditions of stars in the equatorial region

$$Y\left(\xi, \frac{\pi}{2}\right) = 0, \quad \frac{\partial}{\partial \xi} Y\left(\xi, \frac{\pi}{2}\right) = 0 \quad (10)$$

determine the maximal permissible value of the parameter  $\Omega_{\max}$  and the corresponding value of the equatorial radius  $\xi_e^{\max}$ . According to definition (7), only positive solutions of Eq. (8) have a physical meaning, which is the two-dimensional differential equation of the second order in partial derivatives with a dimensionless parameter  $\Omega \geq 0$ .

Eq. (8) is similar to the Poisson equation, therefore it can formally be considered as the equation for dimensionless gravitational potential, which is created by the dimensionless density distribution  $(4\pi)^{-1} \cdot \{\Omega^2 - Y(\xi, \theta)\}$ . In this regard, this equation can be rewritten in the integral form

$$Y(\xi, \theta) = 1 + \sum_{l=1}^{\infty} C_{2l} \xi^{2l} P_{2l}(t) - \frac{1}{4\pi} \int \{\Omega^2 - Y(\xi', \theta')\} Q(\xi, \xi') d\xi', \quad (11)$$

where  $C_{2l}$  are integration constants,  $P_{2l}(t)$  are the Legendre polynomials of the  $2l$ -th order, the kernel of the equation is

$$Q(\xi, \xi') = |\xi - \xi'|^{-1} - (\xi')^{-1}, \quad (12)$$

and the integration is performed over the stellar volume. Taking into account the identity

$$\Delta_{\xi, \theta} \{\xi^l P_l(t)\} = 0, \quad (13)$$

it is easy to verify that Eqs. (8) and (11) are equivalent.

The gravitational potential inside a star (3) is related to dimensionless potential

$$\Phi(\xi) = -\frac{1}{4\pi} \int \frac{Y(\xi')}{|\xi - \xi'|} d\xi' \quad (14)$$

as follows

$$\Phi_{\text{grav}}(\mathbf{r}) = 4\pi G \lambda^2 \rho_c \Phi(\xi). \quad (15)$$

Rewriting Eq. (2) in dimensionless variables, we obtain the relation

$$\frac{\partial}{\partial \xi} \left\{ \Phi_n(\xi, \theta) + Y(\xi, \theta) \right\} = \frac{\Omega^2}{3} \xi \left\{ 1 - P_2(t) \right\}. \tag{16}$$

Eq. (11) can be represented in terms  $Y(\xi, \theta)$ ,  $\Phi_n(\xi, \theta)$ , namely

$$Y(\xi, \theta) + \{ \Phi(\xi, \theta) - \Phi(0, 0) \} = 1 + \sum_{l=1} C_{2l} \xi^{2l} P_{2l}(t) + \Omega^2 \{ \Phi_0(\xi, \theta) - \Phi_0(0, 0) \}, \tag{17}$$

where  $\Phi_0(\xi, \theta)$  determines expression (14) at  $Y(\xi') \equiv 1$ . This allows us to convert Eq. (16) to a form

$$\frac{\partial}{\partial \xi} \left\{ \sum_{l=1} C_{2l} \xi^{2l} P_{2l}(t) + \Omega^2 [\Phi_0(\xi, \theta) - \Phi_0(0, 0)] \right\} = \xi \frac{\Omega^2}{3} \left( 1 - P_2(t) \right). \tag{18}$$

The difference of potentials  $\Phi_0(\xi, \theta) - \Phi_0(0, 0)$  is easy to calculate using an expansion in the series of kernel  $Q(\xi, \xi')$  for the Legendre polynomials and performing integration over the variable  $0 \leq \xi' \leq \xi_0(t)$ , where  $\xi_0(t)$  is the root of the equation  $Y(\xi, \theta) = 0$ . It determines the equation of the polytrope surface. In this way we find that

$$\begin{aligned} \Phi_0(\xi, \theta) - \Phi_0(0, 0) &= -\frac{1}{4\pi} \int d\xi' Q(\xi, \xi') = \frac{\xi^2}{6} + \frac{\xi^2}{2} P_2(t) I_2 + \sum_{l=2}^{\infty} \xi^{2l} P_{2l}(t) I_{2l}, \\ I_2 &= -\int_{-1}^1 P_2(t') \ln \xi_0(t') dt', \quad I_{2l} = \frac{1}{4} (l-1)^{-1} \int_{-1}^1 P_{2l}(t') (\xi_0(t'))^{2-2l} dt' \quad \text{at } l \geq 2. \end{aligned} \tag{19}$$

We note that  $I_{2l} = 0$  at  $l \geq 2$ , where the star is approximated by the rotational ellipsoid (Chandrasekhar, 1969). Substituting expression (19) into Eq. (18), we get the equality

$$(2C_2 + \Omega^2 I_2) P_2(t) + \sum_{l=2}^{\infty} (C_{2l} + \Omega^2 I_{2l}) 2l \xi^{2l-2} P_{2l}(t) = -\frac{\Omega^2}{3} P_2(t). \tag{20}$$

Given the orthogonality of the Legendre polynomials, it follows that

$$C_2 = -\frac{\Omega^2}{6} \left( 1 + 3I_2 \right), \quad C_{2l} = -\Omega^2 I_{2l} \quad \text{at } l \geq 2. \tag{21}$$

Therefore, Eq. (11) can be written in the form

$$Y(\xi, \theta) = 1 + \frac{\Omega^2 \xi^2}{6} \left( 1 - P_2(t) \right) + \frac{1}{4\pi} \int Y(\xi', \theta') Q(\xi, \xi') d\xi'. \tag{22}$$

Eqs. (8) and (22) are the closed system, which do not require any additional information to determine the general solution  $Y(\xi, \theta)$  that corresponds to the given boundary conditions. We solve this system in a self-consistent way, thus we achieve the correct description of the polytrope surface, in contrast to the works of Milne (1923), Chandrasekhar (1933), and Monaghan & Roxburgh (1965), with an approximate description of the peripheral region.

In our previous work (Vavruk et al., 2019) the approximation is accepted, according to which the polytrope surface is the surface of a rotational ellipsoid with eccentricity  $e$  and the equatorial radius  $\xi_e$ , which were determined self-consistently. In this approximation (Vavruk et al., 2019)

$$\xi_0(t) = \xi_e \left\{ 1 + t^2 \frac{e^2}{1 - e^2} \right\}^{-1/2}, \quad I_2 = I_2(e) = \frac{2}{3} + \frac{1 - e^2}{e^2} - \frac{\sqrt{1 - e^2}}{e^3} \arcsin e. \quad (23)$$

However, such an approximation is only one of the possible calculation variants.

### 3. The solution of the equilibrium equation

Using the substitution

$$Y(\xi, \theta) = \Omega^2 \left\{ \varphi(\xi, \theta) + \frac{\xi^2}{4} \sin^2 \theta \right\} \quad (24)$$

Eq. (8) takes the form

$$\Delta_{\xi, \theta} \varphi(\xi, \theta) + \varphi(\xi, \theta) = -\frac{1}{4} \xi^2 \sin^2 \theta, \quad (25)$$

which does not contain parameter  $\Omega^2$ . In the corresponding homogeneous equation the variables are separated and its general solution reads

$$\varphi(\xi, \theta) = \sum_{l=0}^{\infty} \alpha_{2l} j_{2l}(\xi) P_{2l}(t), \quad (26)$$

where  $j_{2l}(\xi)$  is the spherical Bessel function of the first kind (Abramowitz & Stegun, 1970) and  $\alpha_{2l}$  are integration constants. The particular solution of Eq. (25) we find in the form

$$\varphi_p(\xi, \theta) = \sum_{l=2}^{\infty} b_{2l} [\xi \sin \theta]^{2l-2}. \quad (27)$$

Using the equality

$$\Delta_{\xi, \theta} \{\xi \sin \theta\}^{2l} = (2l)^2 \{\xi \sin \theta\}^{2l-2}, \quad (28)$$

we see that

$$b_{2l} = (-1)^{l-1} 2^{-2l} (l!)^{-2}, \tag{29}$$

therefore

$$\frac{1}{4} \xi^2 \sin^2 \theta + \varphi_p(\xi, \theta) = 1 - J_0(\xi \sin \theta), \tag{30}$$

where  $J_0(z)$  is the Bessel function of the zero order (Abramowitz & Stegun, 1970). From Eq. (8) for the function  $Y(\xi, \theta)$  it follows the asymptotic behavior

$$Y(\xi, \theta) \Rightarrow 1 - \frac{\xi^2}{6} + \frac{\Omega^2 \xi^2}{4} \sin^2 \theta + \dots \tag{31}$$

at  $\xi \rightarrow 0$ ; as a result, the general solution of Eq. (8), which corresponds to the boundary conditions at  $\xi = 0$ , can be represented in the form

$$Y(\xi, \theta) = j_0(\xi) + \Omega^2 \left\{ 1 - J_0(\xi[1 - t^2]^{1/2}) + \sum_{l=1}^{\infty} \alpha_{2l} j_{2l}(\xi) P_{2l}(t) \right\}. \tag{32}$$

The function  $J_0(\xi[1 - t^2]^{1/2})$  has an expansion in the form of the Legendre polynomials ( $t = \cos \theta$ ) and spherical Bessel functions (Abramowitz & Stegun, 1970)

$$J_0(\xi[1 - t^2]^{1/2}) = \sum_{l=0}^{\infty} D_l j_{2l}(\xi) P_{2l}(t), \tag{33}$$

$$D_l = (4l + 1)(2l)! 2^{-2l} (l!)^{-2}.$$

Thereby the solution can be represented in the form of a series for the orthogonal functions

$$\tilde{Y}(\xi, \theta) = j_0(\xi) + \Omega^2 \left\{ 1 - j_0(\xi) + \sum_{l=1}^{\infty} a_{2l} j_{2l}(\xi) P_{2l}(t) \right\}, \tag{34}$$

where  $a_{2l}$  are new integration constants, which are different from  $\alpha_{2l}$ . Such representation is proposed by Vavrukh et al. (2019). In the practical calculations we restricted ourselves to the terms  $1 \leq l \leq 3$ , and integration constants  $a_{2l}$  are determined from Eq. (22).

Formally, taking into account an infinite number of series terms in the form of the Legendre polynomials, representations (32) and (34) are completely equivalent. Functions (32) and (34) are the two representations of the exact general solution of solutions (8) and (22), which correspond to boundary conditions (10). However, in the practical calculations it is necessary to account for a small number of terms. In this case representations (32) and (34) are no longer equivalent. This is due to the features of the angular dependence of the function

$J_0(\xi[1-t^2]^{1/2})$ :

$$\begin{aligned} \lim_{t \rightarrow \pm 1} J_0(\xi[1-t^2]^{1/2}) &= 1; \quad \lim_{t \rightarrow 0} J_0(\xi[1-t^2]^{1/2}) = J_0(\xi); \\ \frac{1}{2} \int_{-1}^{+1} J_0(\xi[1-t^2]^{1/2}) dt &= j_0(\xi). \end{aligned} \quad (35)$$

Thereby the angular dependence of the function

$$Y(\xi, \theta) = j_0(\xi) + \Omega^2 \left\{ 1 - J_0(\xi[1-t^2]^{1/2}) + \sum_{l=1}^{l_0} \alpha_{2l} j_{2l}(\xi) P_{2l}(t) \right\}, \quad (36)$$

and the function

$$\tilde{Y}(\xi, \theta) = j_0(\xi) + \Omega^2 \left\{ 1 - j_0(\xi) + \sum_{l=1}^{\tilde{l}_0} a_{2l} j_{2l}(\xi) P_{2l}(t) \right\} \quad (37)$$

are different approximations of the exact solution of Eqs. (8) or (22). Expression (37) with  $\tilde{l}_0 = 1$ , which is considered by Caimmi (1980), is the roughest of all possible approximations and exactly coincides with Chandrasekhar's approximation. The term  $1 - J_0(\xi[1-t^2]^{1/2})$  is the result of selective summation of the infinite series in formula (37). This term reflects the natural asymmetry of the solution in the polar and equatorial directions. First of all we consider the case of the calculation based on function (32), which is different from all the representations of the solution of the equilibrium equation for the polytrope with  $n = 1$ , which are used by other authors.

We also note that the linear combination

$$aY(\xi, \theta) + b\tilde{Y}(\xi, \theta) \quad (38)$$

at  $a + b = 1$  is also an approximation of the exact solution, which corresponds to the boundary conditions at  $\xi = 0$ .

#### 4. The calculation of integration constants

Substituting expression (36) into Eq. (22) and taking into account that  $j_0(\xi)$  satisfies Eqs. (8) and (22) at  $\Omega = 0$ , as well as the fact that  $J_0(\xi[1-t^2]^{1/2})$  is a particular solution of Eq. (25), we obtain the relation

$$\begin{aligned} \sum_{l=1}^{l_0} \alpha_{2l} j_{2l}(\xi) P_{2l}(t) &= -P_2(t) \frac{\xi^2}{6} \left\{ 1 + 3I_2 \right\} + \\ &+ \frac{1}{4\pi} \sum_{l=1}^{l_0} \alpha_{2l} \int j_{2l}(\xi') P_{2l}(t') Q(\xi, \xi') d\xi'. \end{aligned} \quad (39)$$

We will perform integration over variables  $\xi', t', \varphi'$ , expanding the kernel  $Q(\xi, \xi')$  in a series of the Legendre polynomials

$$\begin{aligned} \frac{1}{4\pi} \sum_{l=1}^{l_0} \alpha_{2l} \int j_{2l}(\xi') P_{2l}(t') Q(\xi, \xi') d\xi' &= \sum_{l=1}^{l_0} \frac{\alpha_{2l}}{4l+1} \frac{P_{2l}(t)}{\xi^{1+2l}} \int_0^\xi (\xi')^{2+2l} j_{2l}(\xi') d\xi' + \\ &+ \frac{1}{2} \sum_{l=1}^{l_0} \alpha_{2l} P_{2l}(t) \xi^{2l} \int_{-1}^{+1} P_{2l}^2(t') dt' \int_\xi^{\xi_0(t')} j_{2l}(\xi') (\xi')^{1-2l} d\xi' + \\ &+ \frac{1}{2} \sum_{l,m=1}^{l_0} \alpha_{2l} P_{2m}(t) \xi^{2m} (1 - \delta_{m,l}) \int_{-1}^{+1} P_{2l}(t') P_{2m}(t') dt' \int_\xi^{\xi_0(t')} j_{2l}(\xi') (\xi')^{1-2m} d\xi', \end{aligned} \tag{40}$$

where  $\delta_{n,l}$  is the Kronecker symbol and  $\xi_0(t')$  is the root of the equation

$$j_0(\xi_0) + \Omega^2 \left\{ 1 - J_0(\xi_0 [1 - t^2]^{1/2}) + \sum_{l=1}^{l_0} \alpha_{2l} j_{2l}(\xi_0) P_{2l}(t) \right\} = 0. \tag{41}$$

Integration over the variable  $\xi'$  is performed in an analytical form using the equation for the function  $j_{2l}(\xi)$  and recurrent formulae for these functions (Abramowitz & Stegun, 1970). Comparing the coefficients of the same power  $\xi^{2l} P_{2l}(t)$  on the left- and right-hand sides of expression (40), we obtain the system of linear equations for the constants  $\alpha_{2l}$

$$\begin{aligned} \alpha_2 S_{2,2} + \alpha_4 S_{2,4} + \dots + \alpha_{2l_0} S_{2,2l_0} &= -\frac{1}{6} (1 + 3I_2); \\ \alpha_2 S_{4,2} + \alpha_4 S_{4,4} + \dots + \alpha_{2l_0} S_{4,2l_0} &= 0; \\ \vdots & \\ \alpha_2 S_{2l_0,2} + \alpha_4 S_{2l_0,4} + \dots + \alpha_{2l_0} S_{2l_0,2l_0} &= 0. \end{aligned} \tag{42}$$

The coefficients  $S_{2l,2l}, S_{2m,2l}, \dots$  are determined by the expressions

$$\begin{aligned} S_{2l,2l} &= \int_0^1 P_{2l}^2(t) \xi_0^{1-2l} j_{2l-1}(\xi_0) dt; \\ S_{2m,2l} &= - \int_0^1 P_{2m}(t) P_{2l}(t) \left\{ \int_{\xi_1}^{\xi_0} (\xi')^{1-2m} j_{2l}(\xi') d\xi' \right\} dt, \end{aligned} \tag{43}$$

where  $\xi_0 \equiv \xi_0(t)$ . At the same time the non-diagonal coefficients  $S_{2m,2l}$  at  $m \neq l$  do not depend on the lower limit of integration over the variable  $\xi'$  and are also

reduced to the single integrals, for example

$$\begin{aligned}
 S_{2,4} &= \int_0^1 P_2(t)P_4(t) \xi_0^{-1} \{j_3(\xi_0) + 2\xi_0^{-1}j_2(\xi_0)\} dt; \\
 S_{2,6} &= \int_0^1 P_2(t)P_6(t) \xi_0^{-1} \{j_5(\xi_0) + 4\xi_0^{-1}j_4(\xi_0) + 8\xi_0^{-2}j_3(\xi_0)\} dt,
 \end{aligned} \tag{44}$$

etc. In the limit of small angular velocities  $\xi_0(t)$  can be replaced by the Emden surface  $\xi_1 = \pi$ , therefore  $I_2 = 0$  (see form. (19))

$$S_{2,2} \Rightarrow (5\xi_1)^{-1}j_1(\xi_1) = (5\xi_1^2)^{-1}, \quad \alpha_2 = \tilde{\alpha}_2 = -\frac{5}{6}\pi^2, \quad \alpha_{2l} \Rightarrow 0 \text{ at } l \geq 2. \tag{45}$$

This limit corresponds to the Milne – Chandrasekhar approximation (Milne, 1923; Chandrasekhar, 1933).

The root of Eq. (41),  $\xi_0(t)$ , depends on the angular velocity, therefore the constants  $\alpha_{2l}$  are also the functions of the parameter  $\Omega$ . The procedure for determining the constants  $\alpha_{2l}$  is performed in two stages. At the first stage of integration over the polytrope volume we approximate its surface by the surface of some auxiliary rotational ellipsoid with the eccentricity  $e(\Omega)$  and the equatorial radius  $\xi_e(\Omega)$ , and  $\xi_0(t)$  we determine from formula (23). The root of the equation at  $t = 1$  determines the polar radius  $\xi_p(\Omega) \equiv \xi_0(1|\Omega)$  and the root at  $t = 0$  yields the equatorial radius  $\xi_e(\Omega) \equiv \xi_0(0|\Omega)$  at  $0 \leq \Omega \leq \Omega_{\max}$ . The equation

$$e^2(\Omega) = 1 - \left[ \frac{\xi_0(1|\Omega)}{\xi_0(0|\Omega)} \right]^2 \tag{46}$$

determines dependence of the eccentricity  $e(\Omega)$  on the angular velocity. The system of Eqs. (42) – (46), in which  $\Omega$  is an independent parameter, determines the dependencies  $e(\Omega)$ ,  $\xi_e(\Omega)$ ,  $\xi_p(\Omega)$  and  $\alpha_{2l}(\Omega)$  on the angular velocity. The system can be solved numerically by the method of successive approximations. The algorithm of successive iterations is as follows. At the initial value  $\Omega_1 \ll 1$  in the zero approximation values of  $\xi_e(\Omega) = \xi_p(\Omega)$  we determine from Eq. (42) at  $\alpha_2 = \tilde{\alpha}_2$ ,  $\alpha_4 = 0$ . Next we find the values  $S_{2l,2l}$ ,  $S_{2m,2l}$  and solve system (42). In the next iteration we find  $\xi_p(\Omega)$  and  $\xi_e(\Omega)$  from Eq. (41) with the help of coefficients  $\alpha_{2l}$  found in a previous step and calculate the eccentricity  $e(\Omega)$ . We calculate again  $S_{2l,2l}$ ,  $S_{2m,2l}$  and etc.

At the second stage of calculation, having already approximately calculated coefficients  $\alpha_{2l}$ , we determine  $\xi_0(t)$  from Eq. (41) and continue the iteration process. It helps us to determine integration constants  $\alpha_{2l}$  more precisely and decrease the calculation errors. The approximation of the polytrope surface by the rotational ellipsoid surface at the first stage allows us to speed up the iteration process. Such approximation has errors, because of the polytrope surface is slightly different from the rotational ellipsoid surface. But at the second

stage these disadvantages are eliminated. As a result, we find the improved constants  $\alpha_{2l}$  as well as the polar and equatorial radii. Now the eccentricity  $e(\Omega)$  is already determined only by the relations between  $\xi_p(\Omega)$  and  $\xi_e(\Omega)$ , and the polytrope surface is slightly different from the surface of the auxiliary ellipsoid with the parameters  $\xi_p(\Omega)$  and  $\xi_e(\Omega)$ . Obtained in this way integration constants and polytrope characteristics are shown in Tab. 1 at  $l_0 = 2$  in approximation (36). The maximal value of the angular velocity is determined from condition

**Table 1.** Dependence of the model characteristics with the polytropic index  $n = 1$  on the angular velocity according to expression (36). Notation:  $\Omega$  is the angular velocity,  $e(\Omega)$  is the eccentricity,  $\xi_p(\Omega)$ ,  $\xi_e(\Omega)$  are the polar and equatorial radii,  $\alpha_2(\Omega)$ ,  $\alpha_4(\Omega)$  are integration constants, and  $\eta(n, \Omega)$ ,  $\zeta(n, \Omega)$  are determined by Eqs. (47).

$\Omega$	$e(\Omega)$	$\xi_p(\Omega)$	$\xi_e(\Omega)$	$\alpha_2(\Omega)$	$\alpha_4(\Omega)$	$\eta(n, \Omega)$	$\zeta(n, \Omega)$
0.01000	0.03181	3.14081	3.14240	-8.22777	0.00823046	1.00023	1.00069
0.02000	0.06357	3.13845	3.14481	-8.23709	0.0329826	1.00092	1.00276
0.03000	0.09529	3.13453	3.14886	-8.25271	0.0744407	1.00207	1.00624
0.04000	0.12692	3.12906	3.15457	-8.27476	0.132918	1.0037	1.01115
0.05000	0.15846	3.12203	3.16198	-8.30344	0.208868	1.00582	1.01755
0.06000	0.18989	3.11347	3.17117	-8.33901	0.302896	1.00845	1.02550
0.07000	0.22120	3.10338	3.18221	-8.38178	0.415783	1.0116	1.03509
0.08000	0.25234	3.09179	3.19519	-8.43219	0.548513	1.01532	1.04643
0.09000	0.28334	3.07869	3.21025	-8.49072	0.702305	1.01962	1.05963
0.10000	0.31417	3.06410	3.22752	-8.55802	0.87867	1.02456	1.07487
0.11000	0.34483	3.04803	3.24720	-8.63483	1.07946	1.03019	1.09234
0.12000	0.37532	3.03048	3.26950	-8.72212	1.30699	1.03655	1.11227
0.13000	0.40567	3.01144	3.29472	-8.82104	1.56409	1.04374	1.13496
0.14000	0.43586	2.99091	3.32318	-8.93307	1.85437	1.05183	1.16077
0.15000	0.46596	2.96885	3.35536	-9.06006	2.18236	1.06093	1.19018
0.16000	0.49598	2.94521	3.39180	-9.20441	2.55395	1.07119	1.22375
0.17000	0.52601	2.91993	3.43328	-9.36930	2.97691	1.08276	1.26226
0.18000	0.55613	2.89289	3.48081	-9.55908	3.46178	1.09589	1.30672
0.19000	0.58648	2.86392	3.53586	-9.77991	4.02346	1.11086	1.35853
0.20000	0.61728	2.83276	3.60061	-10.04100	4.68409	1.1281	1.41973
0.21000	0.64889	2.79896	3.67856	-10.35720	5.47905	1.14825	1.49344
0.22000	0.68197	2.76174	3.77604	-10.75550	6.47174	1.17234	1.58498
0.23000	0.71801	2.71936	3.90695	-11.29530	7.80005	1.20241	1.70508
0.24000	0.76241	2.66599	4.11998	-12.18550	9.9398	1.24456	1.88674
0.24100	0.76815	2.65918	4.15324	-12.32580	10.2704	1.25026	1.91283
0.24200	0.77450	2.65173	4.19196	-12.48960	10.654	1.25657	1.94223
0.24300	0.78185	2.64324	4.23955	-12.69170	11.1232	1.26383	1.97680
0.24400	0.79133	2.63259	4.30595	-12.97500	11.7734	1.27299	2.02181
0.24410	0.79253	2.63127	4.31477	-13.01280	11.8594	1.27411	2.02749
0.24420	0.79382	2.62987	4.32435	-13.05380	11.9526	1.27532	2.03356
0.24430	0.79522	2.62836	4.33488	-13.09900	12.055	1.27661	2.04014
0.24440	0.79676	2.62671	4.34673	-13.14990	12.17	1.27803	2.04741
0.24450	0.79853	2.62484	4.36049	-13.20900	12.3033	1.27962	2.05566
0.24460	0.80067	2.62259	4.37754	-13.28240	12.4681	1.28153	2.06562
0.24470	0.80375	2.61944	4.40267	-13.39080	12.7103	1.28418	2.07971

(10). This is an instability point at which the leakage of matter occurs from the vicinity of the equator.

In our work Vavruk et al. (2019), integration constants  $a_{2l}$  for the approximation  $\tilde{Y}(\xi, \theta)$  at  $\tilde{l}_0 = 3$  were found in a similar way. The values of the polytrope characteristics in this approximation and coefficients  $a_{2l}$  are given in Tab. 2.

## 5. Dependence of the polytrope characteristics with index $n = 1$ on the angular velocity

In Tab. 1 there are also shown the values

$$\eta(\Omega) = M(\Omega)/M(0), \quad \zeta(\Omega) = I(\Omega)/I(0), \quad (47)$$

where  $M(\Omega)$ ,  $I(\Omega)$  denote the mass and the moment of inertia of the rotating polytrope with index  $n = 1$  in the considered approximation, and  $M(0)$  and  $I(0)$  are, respectively, the mass and the moment of inertia of the polytrope without rotation,

$$M(0) = 4\pi^2\lambda^3\rho_c, \quad I(0) = \frac{8}{3}\pi^2(\pi^2 - 6)\lambda^5\rho_c. \quad (48)$$

In Tab. 2 there are shown the coefficients  $a_{2l}$  and the polytrope characteristics in approximation (37) at  $\tilde{l}_0 = 3$ . Dependence of the equatorial radius on the angular velocity in different approximations is illustrated in Fig. 1. Similarly, dependence of the polar radius on the angular velocity in the same approximations is given in Fig. 2. As it can be seen from these Figures, the Milne – Chandrasekhar approximation is applicable in the vicinity  $0 \leq \Omega \lesssim 0.5 \Omega_{\max}$ , where  $\Omega_{\max} = 0.2447\dots$ . The constants  $\alpha_2$  and  $\alpha_4$  have the opposite signs and significantly depend on the angular velocity. In the region  $0 \leq \Omega \leq 0.5 \Omega_{\max}$  the constant  $\alpha_4$  is small, and in the region  $\Omega > 0.5 \Omega_{\max}$  it is close to  $|\alpha_2|$ . Since in the region  $0 \leq \xi \leq \xi_e(\Omega_{\max})$  the functions  $j_2(\xi)$  and  $j_4(\xi)$  are positive, the approximation  $\alpha_4 = 0$  is only applicable in the region of small velocities  $\Omega$ .

Approximation (37) at  $\tilde{l}_0 = 1$  corresponds to the works of Chandrasekhar (1933) and Caimmi (1980). Herewith, in the work of Chandrasekhar (1933) the constant  $\alpha_2$  is determined by expression (45) at  $\xi_1 = \pi$ , and in the work of Caimmi (1980) it is calculated numerically based on the calculation of the change of the gravitational potential caused by the rotation. The critical values of the angular velocity given by the authors are:  $\Omega_{\max} \approx 0.3315$  (Chandrasekhar, 1933) and  $\Omega_{\max} \approx 0.3264\dots$  (Caimmi, 1980). In fact, the results obtained by the latter author improve the results of Chandrasekhar (1933). The approximation of Milne and Chandrasekhar (Milne, 1923; Chandrasekhar, 1933) is also used by Monaghan & Roxburgh (1965) for the description of the inner polytrope region, the radius of which is close to the Emden radius. It is found the maximal value of the velocity  $\Omega_{\max} \approx 0.2755$ . In the work of James (1964) the polytrope characteristics are calculated numerically. The index  $n = 1$  corresponds to  $\Omega_{\max} \approx 0.2891\dots$ . From these comparisons it follows: the more precise calculation, the smaller value of the critical velocity  $\Omega_{\max}$ .

**Table 2.** Dependence of the model characteristics with the polytropic index  $n = 1$  on the angular velocity according to expression (37). Notation is the same as in Tab. 1.

$\Omega$	$e(\Omega)$	$\xi_p(\Omega)$	$\xi_c(\Omega)$	$a_2(\Omega)$	$a_4(\Omega)$	$a_6(\Omega)$	$\eta(n, \Omega)$	$\zeta(n, \Omega)$
0.01000	0.02739	3.14112	3.14230	-8.22784	0.00610775	$-8.02713 \cdot 10^{-6}$	1.00023	1.00062
0.02000	0.05478	3.13971	3.14443	-8.23739	0.02449	-0.000128907	1.00092	1.00249
0.03000	0.08219	3.13734	3.14799	-8.25338	0.055325	-0.000656943	1.00207	1.00563
0.04000	0.10961	3.13402	3.15302	-8.27594	0.0989151	-0.00209575	1.00369	1.01006
0.05000	0.13706	3.12973	3.15955	-8.30523	0.155695	-0.0051788	1.00580	1.01583
0.06000	0.16455	3.12447	3.16765	-8.34151	0.226242	-0.0108998	1.00839	1.02298
0.07000	0.19208	3.11820	3.17737	-8.38505	0.311294	-0.020555	1.01150	1.03158
0.08000	0.21967	3.11092	3.18880	-8.43625	0.411773	-0.0358001	1.01513	1.04172
0.09000	0.24733	3.10259	3.20205	-8.49557	0.52881	-0.0587258	1.01933	1.05351
0.10000	0.27507	3.09318	3.21725	-8.56357	0.663789	-0.0919578	1.02410	1.06707
0.11000	0.30291	3.08266	3.23456	-8.64098	0.818398	-0.13879	1.02951	1.08256
0.12000	0.33087	3.07097	3.25416	-8.72865	0.9947	-0.203359	1.03557	1.10016
0.13000	0.35900	3.05807	3.27632	-8.82768	1.19523	-0.290887	1.04237	1.12011
0.14000	0.38731	3.04388	3.30131	-8.93941	1.42314	-0.408009	1.04994	1.14270
0.15000	0.41586	3.02832	3.32953	-9.06557	1.68239	-0.563239	1.05839	1.16830
0.16000	0.44471	3.01127	3.36147	-9.20840	1.97802	-0.767633	1.06782	1.19736
0.17000	0.47394	2.99259	3.39779	-9.37084	2.31667	-1.03579	1.07834	1.23047
0.18000	0.50367	2.97208	3.43938	-9.55694	2.70721	-1.3874	1.09014	1.26843
0.19000	0.53407	2.94946	3.48752	-9.77240	3.16206	-1.84985	1.10343	1.31232
0.20000	0.56538	2.92430	3.54414	-10.02570	3.69946	-2.46274	1.11855	1.36371
0.21000	0.59802	2.89594	3.61237	-10.33050	4.3481	-3.28708	1.13597	1.42496
0.22000	0.63273	2.86321	3.69793	-10.71110	5.15825	-4.42644	1.15648	1.50007
0.23000	0.67114	2.82368	3.81334	-11.21930	6.23501	-6.09077	1.18158	1.59696
0.24000	0.71852	2.77019	4.00008	-12.01930	7.90279	-8.92229	1.21544	1.73805
0.24100	0.72446	2.76320	4.02826	-12.13670	8.14357	-9.35381	1.21980	1.75727
0.24200	0.73086	2.75562	4.06018	-12.26860	8.41224	-9.84267	1.22449	1.77830
0.24300	0.73793	2.74724	4.09737	-12.42040	8.71955	-10.4124	1.22964	1.80179
0.24400	0.74604	2.73767	4.14281	-12.60320	9.0861	-11.1087	1.23546	1.82894
0.24500	0.75612	2.72593	4.20403	-12.84440	9.5632	-12.0491	1.24249	1.86270
0.24600	0.77450	2.70593	4.33124	-13.32470	10.4868	-14.0363	1.25413	1.92196
0.24601	0.77507	2.70536	4.33555	-13.34070	10.5167	-14.1062	1.25445	1.92369
0.24602	0.77563	2.70481	4.33977	-13.35610	10.5455	-14.1737	1.25477	1.92537
0.24603	0.77626	2.70418	4.34461	-13.37360	10.5784	-14.2512	1.25512	1.92728
0.24604	0.77702	2.70344	4.35043	-13.39470	10.6177	-14.3446	1.25554	1.92955
0.24605	0.77800	2.70249	4.35808	-13.42230	10.669	-14.4675	1.25608	1.93248
0.24606	0.77959	2.70100	4.37053	-13.46670	10.7512	-14.6673	1.25693	1.93714
0.24607	0.78685	2.69478	4.42985	-13.66320	11.1084	-15.5733	1.26065	1.95773

Given the known coefficients  $\alpha_{2l}$ , we can build the polytrope surface using Eq. (41). The meridional polytrope section in approximation (32) is shown in Fig. 3 for two fixed values of the angular velocity  $\Omega_1 = 0.2$  and  $\Omega_2 = 0.2447$ . As it is shown in the Figure, at the angular velocity far from the maximal angular velocity  $\Omega_{\max}$  the curve 1 coincides with crosses which are built according to (23) and (36). However, at the angular velocity  $\Omega_{\max}$ , the real polytrope surface (curve 3) is significantly different from the surface of the auxiliary ellipsoid (23).

The distribution of matter inside the polytrope determines the gravitational

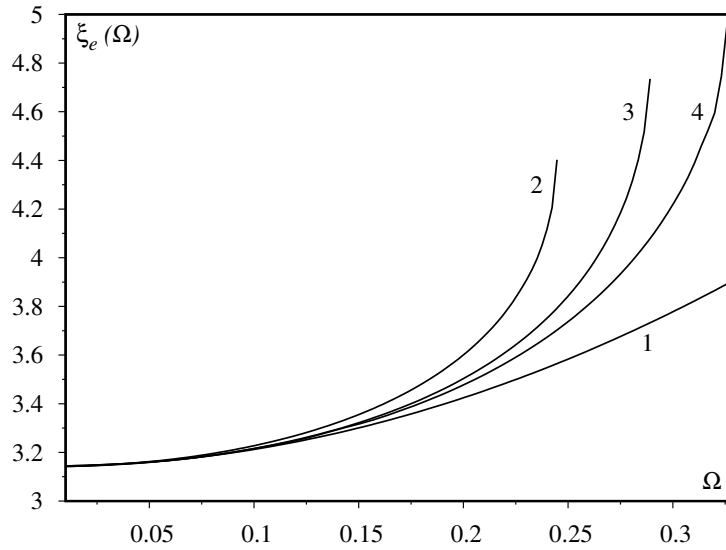


**Figure 1.** Dependence of the equatorial radius  $\xi_e(\Omega)$  on the rotation velocity  $\Omega$  for the polytrope with  $n = 1$  in different approximations. Curve 1 is built on the results of Chandrasekhar (1933), curve 2 corresponds to our approximation (36) at  $l_0 = 2$ . Curve 3 is built on the results of James (1964), curve 4 – on the work of Caimmi (1980).

potential outside it

$$\Phi_{\text{grav}}(\mathbf{r}) = -G \int \frac{d\mathbf{r}' \rho_c}{|\mathbf{r} - \mathbf{r}'|} Y(\xi') = -\frac{GM}{r} \left\{ 1 - \sum_{l=1}^{\infty} P_{2l}(\cos \theta) \left( \frac{\lambda}{r} \right)^{2l} J_{2l}(\Omega) \right\}, \quad (49)$$

where

$$J_{2l}(\Omega) = - \left\{ \int_{-1}^1 dt' \int_0^{\xi_0(t')} d\xi' (\xi')^2 Y(\xi', t') \right\}^{-1} \int_{-1}^1 dt' P_{2l}(t') \int_0^{\xi_0(t')} d\xi' (\xi')^{2l+2} Y(\xi', t'), \quad (50)$$

are the universal dimensionless characteristics, which only depend on the angular velocity  $\Omega$ . Dependence of coefficients  $J_{2l}(\Omega)$  on the angular velocity  $\Omega$  at different values  $l$  according to Tab. 1 is shown in Fig. 4. At the small angular velocities ( $\Omega \leq 0.5 \Omega_{\text{max}}$ ) all coefficients  $J_{2l}(\Omega)$  are small values which are proportional to  $\Omega^2$ . In this region coefficient  $J_2(\Omega)$  is determinative. At the average and rapid angular velocities ( $0.5 \Omega_{\text{max}} \leq \Omega \leq \Omega_{\text{max}}$ ) coefficients  $J_{2l}(\Omega)$  strongly depend on the angular velocity  $\Omega$ .  $|J_{2l}(\Omega)|$  is greater for greater  $l$ .

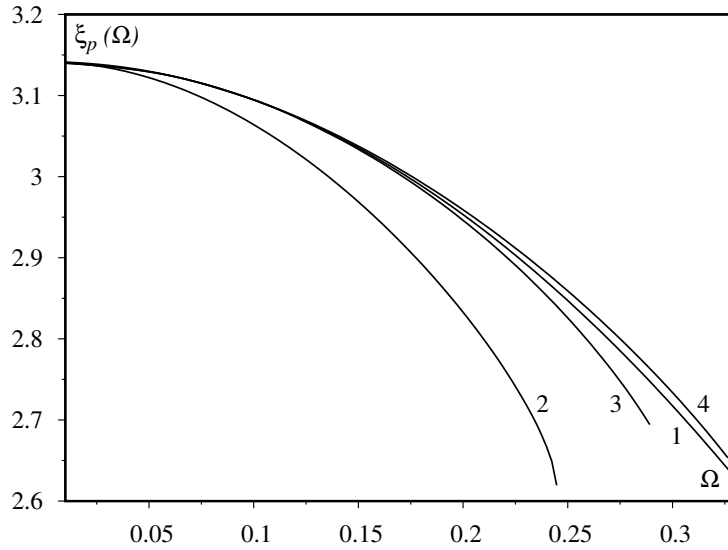


**Figure 2.** Dependence of the polar radius  $\xi_p(\Omega)$  on the rotation velocity  $\Omega$  for the polytrope with  $n = 1$  in different approximations. The notation is the same as in Fig. 1.

### 6. The solution of the equilibrium equation at $n = 1 + \delta$

The model of polytrope with  $n = 1$  is very attractive because in this case we can write the exact solution or its sufficient approximation. However, the polytropic model of a star at  $n = 1$  is still limited, in a general case the polytrope with axial rotation has four independent parameters ( $K, \rho_c, \omega$  and  $n$ ), and the equation of state is written in form (1). Because the polytropic model with  $n = 1$  is a good approximation for massive stars with rapid rotation, it is worth extending it by considering the model with four parameters at  $n = 1 + \delta$ , where  $\delta$  is a small value.

In the dimensionless form the equilibrium equation is written in the form

$$\Delta_{\xi,\theta} Y(\xi, \theta) = \Omega^2 - Y^{1+\delta}(\xi, \theta), \tag{51}$$

and the transition to the dimensionless variables is performed using expressions

$$\begin{aligned} r = \xi \tilde{\lambda}, \quad \rho(r, \theta) = \rho_c Y^{1+\delta}(\xi, \theta), \quad (2 + \delta)K = 4\pi G \tilde{\lambda}^2 \rho_c^\gamma, \\ \gamma = \delta(1 + \delta)^{-1}, \quad \Omega = \omega(2\pi G \rho_c)^{-1/2}. \end{aligned} \tag{52}$$

Analogous to Eq. (22) is now the equation

$$Y(\xi, \theta) = 1 + \frac{\Omega^2 \xi^2}{6} \left(1 - P_2(t)\right) + \frac{1}{4\pi} \int Y^{1+\delta}(\xi', \theta') Q(\xi, \xi') d\xi'. \tag{53}$$

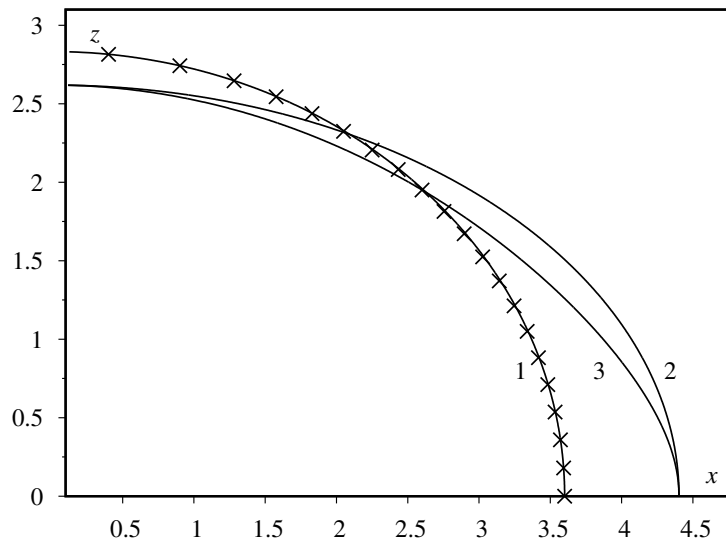


**Figure 3.** The meridional section of the polytrope surface. Curve 1 corresponds to formulae (23) which determine the rotational polytrope surface at the angular velocity  $\Omega_1 = 0.2$ . Curve 2 – the same but for  $\Omega_2 = 0.2447$ . Curve 3 is built according to formula (36) at  $\Omega_2 = 0.2447$ . Crosses are built according to formula (36) at  $\Omega_1 = 0.2$ .

It is obvious from the general physical considerations that  $\tilde{Y}(\xi, \theta)$  is a monotonous function of the polytropic index. Therefore, at  $|\delta| \ll 1$  we can use the iteration method in Eq. (53) and in the zero approximation  $Y(\xi', \theta')$  is replaced by  $Y_1(\xi', \theta')$ , which corresponds to  $\delta = 0$ . The first iteration yields

$$Y(\xi, \theta) = Y_1(\xi', \theta') + \frac{1}{4\pi} \int Q(\xi, \xi') Y_1(\xi', \theta') [Y_1^\delta(\xi', \theta') - 1] d\xi'. \quad (54)$$

In particular, in the linear approximation over the parameter  $\delta$

$$Y(\xi, \theta) = Y_1(\xi', \theta') + \frac{\delta}{4\pi} \int Q(\xi, \xi') Y_1(\xi', \theta') \ln Y_1(\xi', \theta') d\xi'. \quad (55)$$

Expanding the kernel  $Q(\xi, \xi')$  in series of the Legendre polynomials, we obtain the final representation

$$Y(\xi, \theta) = Y_1(\xi, \theta) + \frac{\delta}{2} \left\{ f_0(\xi) + \sum_{l=1}^{\infty} P_{2l}(t) f_{2l}(\xi) \right\}. \quad (56)$$

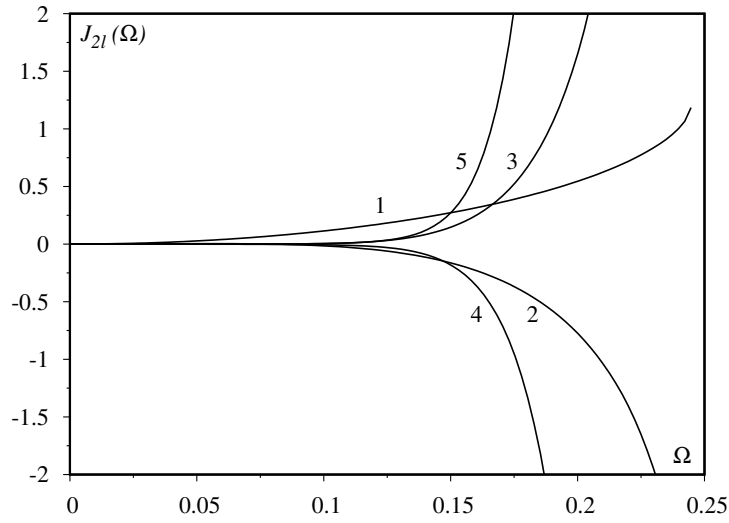


**Figure 4.** Dependence of coefficients (moments of inertia)  $J_{2l}(\Omega)$  on the angular velocity  $\Omega$  for several values of the parameter  $l$  ( $1 \leq l \leq 5$ ,  $\Delta l = 1$ ) (see Eqs. (49), (50)). Curve 1 corresponds to  $J_{2l}(\Omega)$  at  $l = 1$ , curve 5 –  $l = 5$ .

The functions  $f_0(\xi)$  and  $f_{2l}(\xi)$  are determined by the following expressions:

$$\begin{aligned}
 f_0(\xi) &= - \int_0^\xi d\xi' \xi' \int_{-1}^1 dt' \Psi(\xi', t') + \frac{1}{\xi} \int_0^\xi d\xi' (\xi')^2 \int_{-1}^1 dt' \Psi(\xi', t'), \\
 f_{2l}(\xi) &= (\xi)^{-1-2l} \int_0^\xi d\xi' (\xi')^{2l+2} \int_{-1}^1 dt' P_{2l}(t') \Psi(\xi', t') + \\
 &+ \xi^{2l} \int_{-1}^1 dt' P_{2l}(t') \int_\xi^{\xi_0(t')} d\xi' (\xi')^{1-2l} \Psi(\xi', t'); \quad \Psi(\xi', t') = Y_1(\xi', t') \ln [Y_1(\xi', t')].
 \end{aligned}
 \tag{57}$$

A general solution,  $Y(\xi, \theta)$ , according to expression (56) at a fixed value of the angular velocity  $\Omega = 0.2$  is shown in Fig. 5. In this case  $Y_1(\xi, \theta)$  is determined by expression (36). As it is shown in Figure 5 at the positive values  $\delta$  we have the increase of both the equatorial and polar radii. This corresponds to the general behavior of the polytrope radius without rotation when varying the index  $n$ .

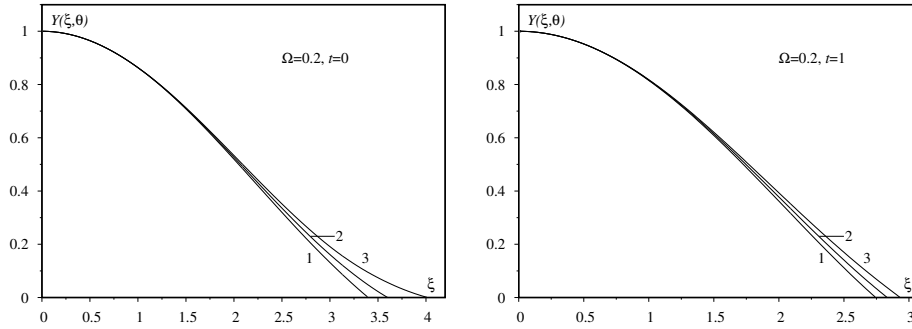


**Figure 5.** A general solution of the equilibrium equation  $Y(\xi, \theta)$  according to the expression (56) at fixed values  $\Omega$  and  $t$ . Curves 1 correspond to the equilibrium equation at  $\delta = -0.1$ , curves 2 –  $\delta = 0$ , curves 3 –  $\delta = 0.1$ .

## 7. The inverse problem for the polytrope with index $n = 1$

The polytrope with  $n = 1$  can be used for the construction of simple polytropic models of stars of early spectral classes, for which significant velocities of angular rotation are typical (Kong et al., 2015). Such a model has three independent parameters  $K$ ,  $\rho_c$ ,  $\omega$ , which have to be determined for the individual observable star. If only the mass  $M$  and the equatorial radius  $R_e$  are reliably known from observations, then we can only find a narrow variation range for model parameters. For example, we consider the model for the star  $\alpha$  Eri ( $M = 9.7466 \cdot 10^{30}$  kg =  $4.9 M_\odot$ ,  $R_e = 8.3520 \cdot 10^9$  m =  $12 R_\odot$ ), the parameters of which are considered in the works of Kong et al. (2015) and Knopik et al. (2017). Taking into account the results of these works, we consider the model in a small variation range of the dimensionless angular velocity  $\Omega_0 \leq \Omega \leq \Omega_{\max}$ . Using the results of our calculations from Tables 1 and 2, for each  $\Omega$  we find the corresponding values  $e(\Omega)$  and  $\xi_e(\Omega)$ . From the relation

$$\frac{M}{R_e^3} = 4\pi^2 \eta(\Omega) \rho_c \xi_e^{-3}(\Omega) \quad (58)$$

we find the density in the stellar centre  $\rho_c(\Omega)$ . From the relation

$$R_e = \xi_e(\Omega) \left( \frac{K}{2\pi G} \right)^{1/2} \quad (59)$$

we determine the parameter  $K$ , and from definition (9) we obtain  $\omega(\Omega)$ . In the work of Kong et al. (2015) the angular velocity was not determined, but there was used its value at the stellar equator obtained from observations with the help of the Doppler effect. Such a value of the angular velocity is bigger than the angular velocity in the polytrope model due to the presence of differential

rotation. For the model with eccentricity  $e = 0.7454$ , which is used by Kong et al. (2015), at  $\Omega = 0.23655$  and the dimensionless equatorial radius  $\xi_e(\Omega) = 4.02993$  in approximation (36), we obtain

$$K_1 = 1.801 \cdot 10^9 \text{ Pa m}^6 (\text{kg})^{-2}, \rho_c^{(1)} = 22.588 \text{ kg m}^{-3}, \omega_1 = 2.302 \cdot 10^{-5} \text{ s}^{-1}. \quad (60)$$

At  $\Omega = 0.24396$  the dimensionless equatorial radius  $\xi_e(\Omega) = 4.12304$  in approximation (37), therefore

$$K_2 = 1.721 \cdot 10^9 \text{ Pa m}^6 (\text{kg})^{-2}, \rho_c^{(2)} = 24.045 \text{ kg m}^{-3}, \omega_2 = 2.450 \cdot 10^{-5} \text{ s}^{-1}. \quad (61)$$

Comparing with the result of Kong et al. (2015) ( $K_0 = 1.75 \cdot 10^9 \text{ Pa m}^6 (\text{kg})^{-2}$ ), we can see that the parameter  $K > K_0$  from approximation (36), and  $K < K_0$  from approximation (37). The approximate solution of the equilibrium equation in the form

$$\frac{3}{8}Y(\xi, \theta) + \frac{5}{8}\tilde{Y}(\xi, \theta) \quad (62)$$

(which is close to the “gold section”), where  $Y(\xi, \theta)$  and  $\tilde{Y}(\xi, \theta)$  are determined by expressions (36) and (37) at  $\Omega = 0.241496$  and  $\xi_e(\Omega) = 4.08559$ , which is calculated numerically, allows us to determine the polytropic parameters

$$K = 1.752 \cdot 10^9 \text{ Pa m}^6 (\text{kg})^{-2}, \rho_c = 23.437 \text{ kg m}^{-3}, \omega = 2.394 \cdot 10^{-5} \text{ s}^{-1}, \quad (63)$$

which almost coincide with those of Kong et al. (2015). To simplify the usage of formula (62), we represented dependencies of the coefficients  $\alpha_{2l}$  and  $a_{2l}$  as the functions of the angular velocity in the form of Padé approximants. Thereby we obtained the analytical dependence of the equilibrium equation solutions on both the coordinates and  $\Omega$ . The deviation of the obtained angular velocity calculated by Kong et al. (2015) from the observed value for  $\alpha$  Eri ( $2.97 \cdot 10^{-5} \text{ s}^{-1}$ ) we can explain with the differential rotation of the stellar surface layers. Based on the found parameters  $K$ ,  $\rho_c$  and  $\Omega$  we calculated coefficients  $J_{2l}(\Omega)$  for the model of  $\alpha$  Eri, which are given in Tab. 3. For the comparison

**Table 3.** Coefficients  $J_{2l}(\Omega)$  for the model of  $\alpha$  Eri for different values of  $l$ .

$l$	1	2	3	4	5
$J_{2l}(\Omega)$	0.934751	-2.65689	11.8846	-68.2954	459.572

with results of Kong et al. (2015), we should replace the length scale  $\lambda$  with the scale  $R_e = 8.3520 \cdot 10^9 \text{ m}$ , writing the potential  $\Phi_{\text{grav}}(\mathbf{r})$  in the form

$$\Phi_{\text{grav}}(\mathbf{r}) = -\frac{GM}{R_e} \frac{1}{\tilde{r}} \left\{ 1 - \sum_{l=1}^{\infty} \frac{P_{2l}(\cos \theta)}{\tilde{r}^{2l}} I_{2l}(\Omega) \right\}, \quad (64)$$

**Table 4.** The parameters  $K$  and  $\rho_c$  of the polytropic model according to the averaged rotational velocities of main-sequence stars. (The observable values  $M$ ,  $R$ ,  $\omega$  are taken from the work of McNally (1965)).

Sp	$M, 10^{30}\text{kg}$	$R, 10^9\text{m}$	$\omega, 10^{-5}\text{s}^{-1}$	$K, 10^9\text{Pa} \cdot \text{m}^6(\text{kg})^{-2}$	$\rho_c, \text{kg}/\text{m}^3$	$\xi_e(\Omega)$	$\Omega$	$\eta(\Omega)$
O5	79	12	1.5	5.69709	38.6225	3.25561	0.118	1.03462
B0	34	5.3	3.8	1.08767	197.267	3.29082	0.133	1.04508
B5	14	2.8	7.6	0.29196	573.682	3.35562	0.155	1.06400
A0	7.1	1.8	10.0	0.12207	1081.91	3.33617	0.149	1.05836
A5	4.4	1.2	13.0	0.055583	2206.65	3.29602	0.135	1.04661
F0	3.5	0.94	10.0	0.036262	3428.6	3.19653	0.084	1.01682
F5	2.8	0.84	3.0	0.029897	3720.64	3.14589	0.024	1.00132
G0	2.1	0.73	1.6	0.022626	4242.68	3.14266	0.012	1.00033

where  $I_{2l}(\Omega) = J_{2l}(\Omega) \cdot (\lambda/R_e)^{2l}$ ,  $\tilde{r} = r/R_e$ . Found in this way  $I_{2l}(\Omega)$  are close to those of Kong et al. (2015). In particular, at  $l = 1$  we obtain  $I_2(\Omega) = 0.05603$ , which differs from that of Kong et al. (2015) by less than 2.4%.

It makes also sense to define approximately the polytropic model parameters for a certain class of stars with rapid rotation. We used the averaged (statistical) values of masses and radii of stars of early spectral classes (O5÷G0) from the work of McNally (1965). Taking the radii, which are given in Tab. 4 as equatorial, we calculated the values of the parameters  $K$  and  $\rho_c$  in approximation (62) for the grid parameters of the values  $\varepsilon = R_p/R_e$ . From this grid we selected results that correspond to those  $\varepsilon$  at which the calculated values  $\omega$  coincide with submitted ones in the work of McNally (1965). Dependence of the parameters of the ‘‘class’’ model  $K$  and  $\rho_c$  on the mass of stars obtained here turned out to be expected: large values of  $K$  (small  $\rho_c$ ) correspond to massive stars in which the density of matter is small; and small values of  $K$  (large  $\rho_c$ ) correspond to low-mass stars in which the central density of matter is large. Although the obtained results are approximate, they illustrate dependence of the polytrope parameters on the spectral class or average stellar mass.

## 8. Conclusions

The polytrope model with  $n = 1$  takes the central place in the polytropic theory with axial rotation. Due to its simplicity it allows us to obtain the solutions of the equilibrium equation with high precision and yields a reliable values of the model characteristics. Therefore, finding the solution of the equilibrium equation of this model in different approximations and their application is one of actual problems of astrophysics. We obtained a simple analytical shape of the solution of the differential equilibrium Eqs. (2), (8) for the polytrope with  $n = 1$  and solid-body rotation in the form of infinite series (32) or (34). Both variants allow approximations in the form of series with a small number of terms (36) and (37), or their linear combinations (38). The practical calculation of the coefficients

$\alpha_{2l}$  were performed based on the integral form of Eq. (22), that is reduced to the system of linear equations (42). The system of Eqs. (41), (42) we solved by a two-stage numerical iteration method. The iteration procedure allows us to calculate simultaneously dependence of the coefficients  $\alpha_{2l}$ , polar and equatorial radii on the dimensionless angular velocity  $\Omega$ . The approximation of the exact solution, which is obtained explicitly, allows us to calculate dependence of the mass and the moment of inertia on the angular velocity. In an analogous way we find the constants  $a_{2l}$ , geometrical and physical characteristics of the model as the functions of  $\Omega$  in approximation (37). As it can be seen in Figures and Tables 1 and 2, the critical value of the angular velocity  $\Omega_{\max}$  is smaller than in the work of other authors. Approximation (36) is used for the calculation of the gravitational potential outside the polytrope. Expansions (36) and (37) have good convergence and the increase in the number of series terms leads to insignificant changes of the characteristics only in the vicinity of  $\Omega_{\max}$ . The convergence of series (36) and (37) is provided by the Bessel functions, which have standard asymptotics at  $\xi \rightarrow 0$  (Abramowitz & Stegun, 1970). However, it strongly depends on the angular velocity. For example, for the case of the equator from approximation (37) the ratio of individual terms of the series can be represented as

$$\begin{aligned} f_2 : f_4 : f_6 &= 1.31 : 0.02 : 0.002 \quad \text{at} \quad \Omega = 0.1, \\ f_2 : f_4 : f_6 &= 1.53 : 0.12 : 0.007 \quad \text{at} \quad \Omega = 0.2, \\ f_2 : f_4 : f_6 &= 1.44 : 0.64 : 0.13 \quad \text{at} \quad \Omega = \Omega_{\max}, \end{aligned}$$

where  $f_{2l} = a_{2l}(\Omega)P_{2l}(0)j_{2l}(\xi_e)$ , ( $1 \leq l \leq 3$ ). It can be seen that in an almost entire domain of the angular velocity the convergence is very good, but it worsens in the vicinity of  $\Omega_{\max}(1)$ . Obviously, finding the solutions of the equilibrium equation in the vicinity of  $\Omega_{\max}$  deserves special attention.

With all its advantages the model with  $n = 1$  is only one of the polytropic models, which can be used for the description of celestial objects. Therefore, it is appropriate to have precise enough solutions of the mechanical equilibrium equation for the model with  $n \neq 1$ . The solution of the equilibrium equation for the case  $n = 1 + \delta$  (where  $\delta$  is a small value) was obtained by the method of the perturbation theory. Dependence of the surface shape of such a polytrope on the parameter  $\delta$  corresponds to the famous dependence of the polytrope characteristics on the index  $n$  (Chandrasekhar, 1933). This model can be useful for the description of stars with the very rapid angular velocity ( $\Omega \geq 0.25$ ).

The geometrical and physical characteristics of the polytropic models determine not only the solution of the mechanical equilibrium in the dimensionless form, but also the values of the parameters  $K$ ,  $\rho_c$ ,  $\omega$  for the individual celestial bodies. Therefore, the inverse problem of the theory arises – finding these parameters according to the known solution of the equilibrium equation and observable characteristics of celestial bodies. As an illustration of our approach we considered the problem of the parameters of the polytropic model for the

star  $\alpha$  Eri and compared them with the results of the work of Kong et al. (2015). In approximation (62) the value  $K = 1.752 \cdot 10^9 \text{ Pa m}^6 (\text{kg})^{-2}$  obtained by us almost coincides with that of Kong et al. (2015). Coefficients  $J_{2l}(\Omega)$  are calculated in approximation (62), which are also close to the coefficients of Kong et al. (2015). Moreover, for the first time, we considered the problem of the approximate calculation of the parameters  $K$  and  $\rho_c$  for the full subclasses of stars, namely O5 $\div$ G0, using the observable data from the work of McNally (1965).

The considered examples indicate that the simple analytical approximations of the solution of the equilibrium equation obtained by us are useful for the description of celestial bodies, in particular to build stellar models with rapid axial rotation.

## References

- Abramowitz, M. & Stegun, I. A. 1970, *Handbook of mathematical functions: with formulas, graphs, and mathematical tables*
- Caimmi, R., Emden-Chandrasekhar Axisymmetric Solid-Body Rotating Polytropes - Part One - Exact Solutions for the Special Cases  $N=0, 1$  and  $5$ . 1980, *Astrophysics and Space Science*, **71**, 415, DOI: 10.1007/BF00639402
- Chandrasekhar, S., The Maximum Mass of Ideal White Dwarfs. 1931, *Astrophysical Journal*, **74**, 81, DOI: 10.1086/143324
- Chandrasekhar, S., The equilibrium of distorted polytropes. I. The rotational problem. 1933, *Monthly Notices of the RAS*, **93**, 390, DOI: 10.1093/mnras/93.5.390
- Chandrasekhar, S. 1969, *Ellipsoidal figures of equilibrium*
- Eddington, A. S. 1926, *The Internal Constitution of the Stars*
- Emden, R. 1907, *Gaskugeln: Anwendungen der mechanischen Wärmetheorie auf kosmologische und meteorologische Probleme*
- Fowler, R. H., Emden's equation: The solutions of Emden's and similar differential equations. 1930, *Monthly Notices of the RAS*, **91**, 63, DOI: 10.1093/mnras/91.1.63
- James, R. A., The Structure and Stability of Rotating Gas Masses. 1964, *Astrophysical Journal*, **140**, 552, DOI: 10.1086/147949
- Knopik, J., Mach, P., & Odrzywólek, A., The shape of a rapidly rotating polytrope with index unity. 2017, *Monthly Notices of the RAS*, **467**, 4965, DOI: 10.1093/mnras/stx164
- Kong, D., Zhang, K., & Schubert, G., An exact solution for arbitrarily rotating gaseous polytropes with index unity. 2015, *Monthly Notices of the RAS*, **448**, 456, DOI: 10.1093/mnras/stu2759

- Kopal, Z., Bemerkung zur Theorie der rotierenden Polytropen. 1937, *Zeitschrift fuer Astrophysik*, **14**, 135
- Lane, H. J., On the theoretical temperature of the Sun, under the hypothesis of a gaseous mass maintaining its volume by its internal heat, and depending on the laws of gases as known to terrestrial experiment. 1870, *American Journal of Science*, **50**, 57, DOI: 10.2475/ajs.s2-50.148.57
- McNally, D., The distribution of angular momentum among main sequence stars. 1965, *The Observatory*, **85**, 166
- Milne, E. A., The equilibrium of a rotating star. 1923, *Monthly Notices of the RAS*, **83**, 118, DOI: 10.1093/mnras/83.3.118
- Monaghan, J. J. & Roxburgh, I. W., The structure of rapidly rotating polytropes. 1965, *Monthly Notices of the RAS*, **131**, 13, DOI: 10.1093/mnras/131.1.13
- Vavrukh, M. V., Smerechynskiy, S. V., & Tyshko, N. L., The microscopic parameters and the macroscopic characteristics of real degenerate dwarfs. 2010, *Journal of Physical Studies*, **14**, 4901, DOI: 10.30970/jps.14.4901
- Vavrukh, M. V., Tyshko, N. L., Dzikovskyi, D. V., & Stelmakh, O. M., The self-consistent description of stellar equilibrium with axial rotation. 2019, *Mathematical Modeling and Computing*, **6**, 153, DOI: 10.23939/mmc2019.02.153

## Substellar and stellar companions in eclipsing binaries

K. Zervas, E.-P. Christopoulou and A. Papageorgiou

*Department of Physics, University of Patras, 26500 Patras, Greece  
(E-mail: konst.zervas@upatras.gr)*

Received: September 4, 2020; Accepted: September 29, 2020

**Abstract.** We present an extensive analysis of O-C diagrams constructed by previously published times of minima and updated by photometric observations carried out at Mythodea Observatory (Astrophysics Laboratory, Department of Physics, University of Patras). A two-companion model is attributed to the over-contact (W UMa type) binary system TZ Boo according to a Light-Time Effect (LITE), while in the case of the post-common envelope binary NSVS 14256825 a Jovian type circumbinary companion is the most plausible explanation of the apparent period variation.

**Key words:** binaries: eclipsing – binaries (including multiple): close – planetary systems

### 1. Introduction

The apparent cyclical period variation of an eclipsing binary can provide an indirect evidence of a circumbinary companion as a result of gravitational attraction (Light-Time Effect, LITE; Irwin, 1952) or might instead be due to stellar magnetic activity (Applegate, 1992).

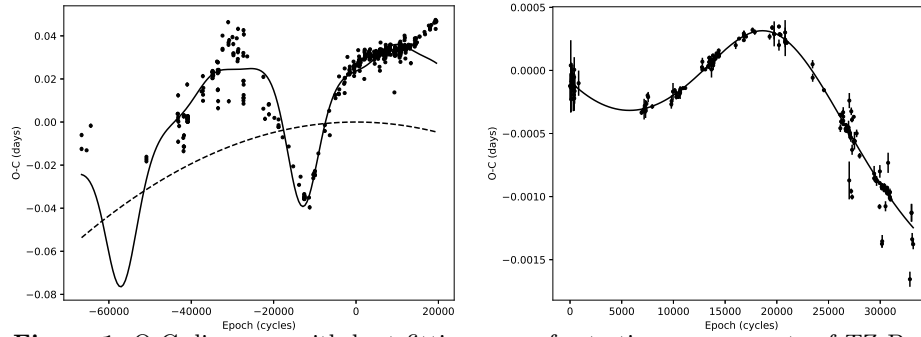
### 2. O-C diagram analysis

We implement a series of optimization techniques which consist of a first solution determination using Nelder-Mead Downhill Simplex and Levenberg-Marquardt algorithms, while the globality of solution (lowest  $\chi^2$ ) is sought by a Heuristic Scanning scheme which implements the two aforementioned methods with a parameter kicking or by a Genetic Algorithm (PIKAIA; Charbonneau, 1995).

As a last step of scanning the topology of  $\chi^2$  parameter space and in order to acquire more realistic parameter value errors we implement a Metropolis-Hastings MCMC algorithm.

**Table 1.** Orbital parameters of tertiary companions for TZ Boo and NSVS 14256825 according to M-H MCMC.

Parameter	TZ Boo	NSVS 14256825
$e_3$	$0.81 \pm 0.02$	$0.03 \pm 0.02$
$A$ (days)	$0.025 \pm 0.001$	$0.0005 \pm 0.0010$
$\omega_3$ (rad)	$5.92 \pm 0.01$	$2.92 \pm 0.01$
$gmt = dP/2dE$ (days cycle $^{-1}$ )	$-0.12 \pm 0.01 \times 10^{-10}$	...
$P_3$ (years)	$35.81 \pm 0.11$	$10.38 \pm 0.12$
$T_3$ (HJD)	$2448510.51 \pm 0.01$	$2456358.95 \pm 0.01$
$P_{bin}$ (days)	$0.29715974 \pm 2.6 \times 10^{-8}$	$0.11037416 \pm 2.1 \times 10^{-8}$
$T_0$ (HJD)	$2452500.16 \pm 0.01$	$245274.21 \pm 0.01$
$M_3$ (coplanar)	$0.84 M_{\odot}$	$16 M_{Jup}$

**Figure 1.** O-C diagrams with best fitting curve for tertiary components of TZ Boo and NSVS 14256825.

In case of TZ Boo the O-C residuals reveal a secondary companion, however, magnetic activity cannot be ruled out as a possible contribution since the energy threshold of Applegate mechanism is relatively small  $\Delta E/E_{sec} = 0.12$  (Applegate, 1992) and  $\Delta E/E_{sec} = 0.1$  (Tian et al., 2009).

## References

- Applegate, J. H., A Mechanism for Orbital Period Modulation in Close Binaries. 1992, *Astrophysical Journal*, **385**, 621, DOI: 10.1086/170967
- Charbonneau, P., Genetic Algorithms in Astronomy and Astrophysics. 1995, *Astrophysical Journal Supplement*, **101**, 309, DOI: 10.1086/192242
- Irwin, J. B., The Determination of a Light-Time Orbit. 1952, *Astrophysical Journal*, **116**, 211, DOI: 10.1086/145604
- Tian, Y. P., Xiang, F. Y., & Tao, X., Period investigation of two RS CVn-type binary stars: RU Cancri and AW Herculis. 2009, *Astrophysics and Space Science*, **319**, 119, DOI: 10.1007/s10509-008-9975-4

## What we can learn from eclipsing binaries in large surveys: The case of EA Catalina systems

A. Papageorgiou<sup>1,2</sup>, P.-E. Christopoulou<sup>3</sup>, M. Catelan<sup>1,2</sup>,  
A.J. Drake<sup>4</sup> and S.G. Djorgovski<sup>4</sup>

<sup>1</sup> *Millennium Institute of Astrophysics, Santiago, Chile*

<sup>2</sup> *Pontificia Universidad Católica de Chile, Santiago, Chile*

<sup>3</sup> *Department of Physics, University of Patras, Greece*

<sup>4</sup> *California Institute of Technology, 1200 East California, USA*

Received: September 4, 2020; Accepted: September 28, 2020

**Abstract.** With the recent availability of large-scale multi-epoch photometric datasets, we were able to study EBs en masse. Large samples are useful to determine not only statistical properties but for finding strange and curious systems that no one had ever studied before, binaries with peculiarities that may reveal physical significance. We present an updated and more detailed catalog of 4680 Northern EAs in the Catalina Sky Survey (CSS). This work includes, new systems, revised period determination and ephemerides, system morphology classification based on machine learning techniques, computation of principal physical parameters with the EBAI (Eclipsing Binary via Artificial Intelligence) and detection of eclipse timing variations. We identify several groups of interesting systems including those with low mass K and M dwarfs, systems with longterm modulation of the maximum brightness, systems with longterm period modulation, potential triple systems and systems with magnetic activity.

**Key words:** large surveys – eclipsing binaries - data analysis

### 1. Introduction

Sky surveys represent a fundamental data basis for Eclipsing Binaries (EBs) since they can generate large, statistical samples or can be used to discover or generate samples of rare or unusual objects, and may lead to discoveries of some previously unknown types. In particular EBs with Algol type light curve (LC) morphology (EAs) provide a good chance not only to determine the fundamental physical properties of stars but also to investigate the interaction between the components, mass transfer, magnetic breaking and the presence of tertiary companions. All these processes play a significant role in the understanding of the origin, evolution and death of close binaries components. Another important feature of EA type systems is that they contain low-mass stars. We continue to exploit the northern data from Catalina Sky Surveys (CSS) spanning 12 yrs, (Drake et al., 2014) searching for and investigating the period variations among

4683 EAs. These were described recently by Papageorgiou et al. (2018), who revised the period, determined the phenomenological parameters of the LCs and classified the systems morphology into detached/semidetached subclasses based on machine-learning techniques.

From this sample Papageorgiou et al. (2019) by applying the Eclipsing Binaries via Artificial Intelligence (EBAI) Artificial Neural Network (ANN), extracted the physical parameters using for the first time two independent methods, based on the template fitting (Layden, 1998), and the Two-Gaussian Model (Mowlavi et al., 2017). The statistical properties of the physical parameter distributions of the above sample were similar to those characterizing the EB systems in the first release of the Kepler catalog of detached EBs (Prša et al., 2011) obtained by the method of neural networks and also with the catalog of parameter values for 257 detached double-lined EBs (Eker et al., 2014) obtained by the traditional method.

One of the well-known methods for the identification of period trends is based on the analysis of the eclipse timing variations (ETVs) of the binary, also called an O-C diagram.

## 2. Basic steps of the analysis

From the latter sample all LCs were cleaned by using a sigma clipping algorithm and the times were converted into Heliocentric Julian Date (HJD). We investigated only those systems whose LCs contain more than 400 points.

To determine times of minima (TOM) we used phase folded and binned LCs of  $\sim 300$  d, using the initial periods from Papageorgiou et al. (2018). In the next step we formed a Gaussian template function for the primary and the secondary eclipses and searched for the best fitting parameters using the method of Nelder-Mead Downhill Simplex and a Markov Chain Monte Carlo (MCMC) procedure for the TOM error calculation.

In order to check that the above computation of ToM can emerge systems with period variations, we run successfully two tests, the first one on a synthetic detached LC generated using PHOEBE 2.0 engine (Prša et al., 2016) with a third component and the second on VY Cet, a well-known EB with period variations, using the LC from the All Sky Automated Survey (ASAS; Pojmanski et al., 2005). We run also a test on the TOM error calculation by evaluating the uncertainties from the LC phenomenological parameters given by Papageorgiou et al. (2018) and Eq. 1 of Pribulla et al. (2012) for the primary and secondary eclipses.

Only EBs with calculated ToM  $\geq 6$  minima were accepted for the O-C analysis. This selection resulted in 2604 EBs. By using the new TOM we updated the linear ephemeris for each EB and constructed the O-C diagram. These were fitted with a sinusoidal or/and a parabolic function using the Levenberg-Marquardt algorithm and the goodness of the solution was tested by applying

a Bayesian Information Criterion (BIC), eliminating the number of EBs with potential period variations in 577 systems. After visual inspection, in the last stage, we accepted only sinusoidal variations with mean ToM error-to-amplitude ratio greater than 1.5 or parabolic variations with period changes greater than  $10^{-10}$  d cycle $^{-1}$ . Fig. 1 shows a representative example of the analysis and fitting of an EB with period variation.

### 3. Results

We have found 126 candidates EBs with period variations, among which we identified 63 EBs with cyclic variations and 63 EBs with more likely quadratic behavior. For the first group assuming that the period modulation is caused by a third companion, we calculated the mass function, the period and the LTTE amplitude (Irwin, 1959) assuming zero eccentricity,  $i_3 = 90^\circ$  and  $M_{12} \sim 2 M_\odot$  and the parameters errors (Papageorgiou & Christopoulou, 2015). In addition, out of these 12 are low-mass candidates (Papageorgiou et al., 2018) and have their initial parameters derived by EBAI or the template method (Papageorgiou et al., 2019) whereas only four have already shown trends of maximum brightness modulation (Papageorgiou et al., 2018).

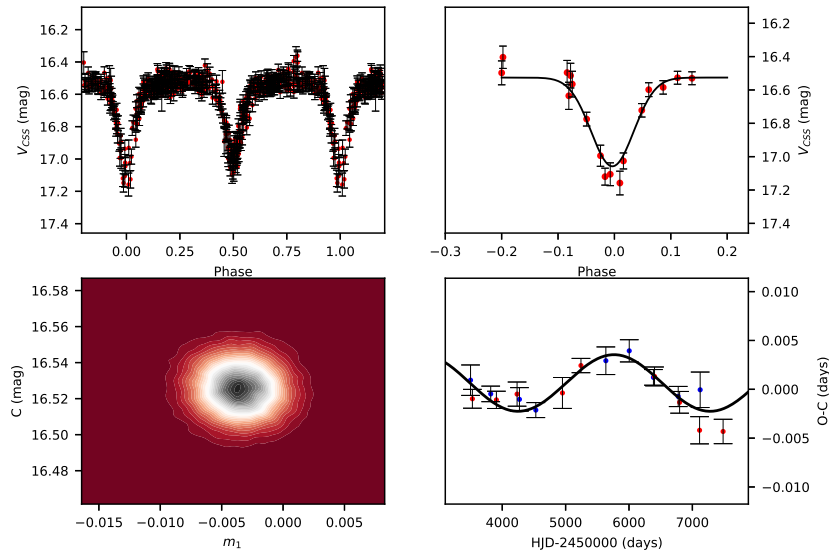


**Figure 1.** Representative example of the O-C analysis and the fitting procedure. The folded LC (upper left panel), the ToM (upper right panel), the MCMC procedure (lower left panel) and the ETV data with a sinusoidal model (lower right panel).

**Acknowledgements.** A.P. and M.C. gratefully acknowledge the support provided by Fondecyt through grants #3160782 and #1171273. Additional support for this project is provided by the Ministry for the Economy, Development, and Tourism's Millennium Science Initiative through grant IC 120009, awarded to the Millennium Institute of Astrophysics (MAS); and by Proyecto Basal AFB-170002.

## References

- Drake, A. J., Graham, M. J., Djorgovski, S. G., et al., The Catalina Surveys Periodic Variable Star Catalog. 2014, *Astrophysical Journal, Supplement*, **213**, 9, DOI: 10.1088/0067-0049/213/1/9
- Eker, Z., Bilir, S., Soydugan, F., et al., The Catalogue of Stellar Parameters from the Detached Double-Lined Eclipsing Binaries in the Milky Way. 2014, *Publications of the Astronomical Society of Australia*, **31**, e024, DOI: 10.1017/pasa.2014.17
- Irwin, J. B., Standard light-time curves. 1959, *Astronomical Journal*, **64**, 149, DOI: 10.1086/107913
- Layden, A. C., RR Lyrae Variables in the Inner Halo. I. Photometry. 1998, *Astronomical Journal*, **115**, 193, DOI: 10.1086/300195
- Mowlavi, N., Lecoœur-Taïbi, I., Holl, B., et al., Gaia eclipsing binary and multiple systems. Two-Gaussian models applied to OGLE-III eclipsing binary light curves in the Large Magellanic Cloud. 2017, *Astronomy and Astrophysics*, **606**, A92, DOI: 10.1051/0004-6361/201730613
- Papageorgiou, A., Catelan, M., Christopoulou, P.-E., Drake, A. J., & Djorgovski, S. G., An Updated Catalog of 4680 Northern Eclipsing Binaries with Algol-type Light-curve Morphology in the Catalina Sky Surveys. 2018, *Astrophysical Journal, Supplement*, **238**, 4, DOI: 10.3847/1538-4365/aad8a9
- Papageorgiou, A., Catelan, M., Christopoulou, P.-E., Drake, A. J., & Djorgovski, S. G., Physical Parameters of Northern Eclipsing Binaries in the Catalina Sky Survey. 2019, *Astrophysical Journal, Supplement*, **242**, 6, DOI: 10.3847/1538-4365/ab13b8
- Papageorgiou, A. & Christopoulou, P. E., Absolute Parameters and Physical Nature of the Low-amplitude Contact Binary HI Draconis. 2015, *Astronomical Journal*, **149**, 168, DOI: 10.1088/0004-6256/149/5/168
- Pojmanski, G., Pilecki, B., & Szczygiel, D., The All Sky Automated Survey. Catalog of Variable Stars. V. Declinations 0 arc - +28 arc of the Northern Hemisphere. 2005, *Acta Astron.*, **55**, 275
- Pribulla, T., Vaňko, M., Ammler-von Eiff, M., et al., The Dwarf project: Eclipsing binaries - precise clocks to discover exoplanets. 2012, *Astronomische Nachrichten*, **333**, 754, DOI: 10.1002/asna.201211722
- Prša, A., Batalha, N., Slawson, R. W., et al., Kepler Eclipsing Binary Stars. I. Catalog and Principal Characterization of 1879 Eclipsing Binaries in the First Data Release. 2011, *Astronomical Journal*, **141**, 83, DOI: 10.1088/0004-6256/141/3/83

Prša, A., Conroy, K. E., Horvat, M., et al., Physics Of Eclipsing Binaries. II. Toward the Increased Model Fidelity. 2016, *Astrophysical Journal, Supplement*, **227**, 29, DOI: 10.3847/1538-4365/227/2/29



PRÁCE ASTRONOMICKÉHO OBSERVATÓRIA  
NA SKALNATOM PLESE  
L, číslo 4

Zostavovateľ:	RNDr. Richard Komžík, CSc.
Vedecký redaktor:	RNDr. Augustín Skopal, DrSc.
Vydal:	Astronomický ústav SAV, Tatranská Lomnica
IČO vydavateľa:	00 166 529
Periodicita:	3-krát ročne
ISSN (on-line verzia):	1336-0337
CODEN:	CAOPF8
Rok vydania:	2020
Počet strán:	68

Contributions of the Astronomical Observatory Skalnaté Pleso are processed using  
 $\LaTeX 2_{\epsilon}$  CAOSP DocumentClass file 3.08 ver. 2020.